Plasmon-polariton waves guided by thin lossy metal films of finite width: Bound modes of symmetric structures

Pierre Berini*
University of Ottawa, School of Information Technology and Engineering, 161 Louis Pasteur Street, P.O. Box 450, Stn. A, Ottawa, Ontario, Canada K1N 6N5
(Received 17 August 1999)

The purely bound electromagnetic modes of propagation supported by symmetric wave guide structures comprised of a thin lossy metal film of finite width embedded in an infinite homogeneous dielectric have been characterized at optical wavelengths. The modes supported are divided into four families depending on the symmetry of their fields. In addition to the four fundamental modes that exist, numerous higher order ones are supported as well. A nomenclature suitable for identifying all modes is discussed. The dispersion of the modes with film thickness and width has been assessed and the effects of varying the background permittivity on the characteristics of the modes determined. The frequency dependence of one of the modes has been investigated. The higher order modes have a cutoff width, below which they are no longer propagated and some of the modes have a cutoff thickness. One of the fundamental modes supported by the structure exhibits very interesting characteristics and is potentially quite useful. It evolves with decreasing film thickness and width towards the transverse electromagnetic (TEM) wave supported by the background (an evolution similar to that exhibited by the s_b mode in symmetric metal film slab wave guides), its losses and phase constant tending asymptotically towards those of the TEM wave. Attenuation values can be well below those of the s_b mode supported by the corresponding metal film slab wave guide. Low mode power attenuation in the neighborhood of 10 to 0.1 dB/cm is achievable at optical communications wavelengths, with even lower values being possible. Carefully selecting the film's thickness and width can make this mode the only long-ranging one supported. In addition, the mode can have a field distribution that renders it excitable using an end-fire approach. The existence of this mode renders the finite-width metal film wave guide attractive for applications requiring short propagation distances and two-dimensional field confinement in the transverse plane.

I. INTRODUCTION

At optical wavelengths, the electromagnetic properties of some metals closely resemble those of an electron gas, or equivalently of a cold plasma. Metals that resemble an almost ideal plasma are commonly termed ''noble metals'' and include, among others, gold, silver, and copper. Numerous experiments as well as classical electron theory both yield an equivalent negative dielectric constant for many metals when excited by an electromagnetic wave at or near optical wavelengths.[1,2] In a recent experimental study, the dielectric function of silver has been accurately measured over the visible optical spectrum and a very close correlation between the measured dielectric function and that obtained via the electron gas model has been demonstrated.[3]

It is a well-known fact that the interface between semi-infinite materials having positive and negative dielectric constants can guide transverse magnetic (TM) surface waves. In the case of a metal-dielectric interface at optical wavelengths, these waves are termed plasmon-polariton modes and propagate as electromagnetic fields coupled to surface plasmons (surface plasma oscillations) comprised of conduction electrons in the metal.[4]

A metal film of a certain thickness bounded by dielectrics above and below is often used as an optical slab (planar, infinitely wide) wave guiding structure, with the core of the wave guide being the metal film. When the film is thin enough, the plasmon-polariton modes guided by the interfaces become coupled due to field tunneling through the metal, thus creating supermodes that exhibit dispersion with metal thickness. The modes supported by infinitely wide symmetric and asymmetric metal film structures are well known, as these structures have been studied by numerous researchers; some notable published works include Refs. 4–10.

In general, only two purely bound TM modes, each having three field components, are guided by an infinitely wide metal film wave guide. In the plane perpendicular to the direction of wave propagation, the electric field of the modes is comprised of a single component, normal to the interfaces and having either a symmetric or asymmetric spatial distribution across the wave guide. Consequently, these modes are denoted s_b and a_b modes, respectively. The s_b mode can have a small attenuation constant and is often termed a long-range surface plasmon-polariton. The fields related to the a_b mode penetrate further into the metal than in the case of the s_b mode and can be much lossier by comparison. Interest in the modes supported by thin metal films has recently intensified due to their useful application in optical communications devices and components. Metal films are commonly employed in optical polarizing devices[11] while long-range surface plasmon-polaritons can be used for signal transmission.[7] In addition to purely bound modes, leaky modes are also known to be supported by these structures.

Infinitely wide metal film structures, however, are of limited practical interest since they offer one-dimensional (1D) field confinement only, with confinement occuring along the

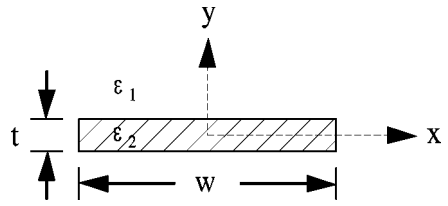

FIG. 1. Wave guide structure considered in this study. The core is comprised of a lossy metal film of thickness t, width w, and permittivity ϵ_2 embedded in a cladding or background consisting of an infinite homogeneous dielectric having a permittivity ϵ_1.

vertical axis perpendicular to the direction of wave propagation implying that modes will spread out laterally as they propagate from a point, source used as the excitation. Metal films of finite width offer 2D confinement in the transverse plane and may be useful for signal transmission and routing or to construct passive components such as couplers and power splitters if suitable low-loss wave guides can be fabricated. Furthermore, metal films of finite width are in fact currently being proposed in polarizing devices,[12] though their fundamental wave guiding characteristics have yet to be determined.

The purpose of this paper is to present a comprehensive description of the purely bound modes of propagation supported by symmetric wave guide structures comprised of a thin lossy metal film of finite width as the core, embedded in an infinite homogeneous dielectric medium, and to investigate the evolution of modes due to variations in the physical parameters of the wave guides. (Preliminary results of this study have already been reported as a short communication.[13]) The paper is organized as follows. Section II summarizes the physical basis and numerical technique used to analyze the structures of interest. Section III describes the nature of the purely bound fundamental and higher-order modes, their dispersion and evolution with film thickness, and discusses a recently proposed mode nomenclature suitable for identifying them.[13] Section IV describes the dispersion of modes with film width, Sec. V presents the changes in wave guiding properties caused by varying the background permittivity, and Sec. VI discusses the frequency dependence of mode solutions. Concluding remarks are given in Sec. VII.

II. PHYSICAL BASIS AND NUMERICAL TECHNIQUE

A. Description of the wave guide structure

The structure considered in this paper is shown in Fig. 1. It consists of a metal film of thickness t, width w and equivalent permittivity ϵ_2, surrounded by an infinite homogeneous dielectric of permittivity ϵ_1. The Cartesian coordinate axes used for the analysis are also shown with propagation taking place along the z axis, which is out of the page.

It is assumed in this study that the metal region shown in Fig. 1 can be modeled as an electron gas over the wavelengths of interest. According to classical or Drude electron theory, the complex relative permittivity of the metal region is given by the well-known plasma frequency dispersion relation[4]

$$\epsilon_{r,2}=\left(1-\frac{\omega_p^2}{\omega^2+\nu^2}\right)-j\left(\frac{\omega_p^2\nu}{\omega(\omega^2+\nu^2)}\right), \tag{1}$$

where ω is the excitation frequency, ω_p is the electron plasma frequency, and ν is the effective electron collision frequency, often expressed as $\nu=1/\tau$ with τ defined as the relaxation time of electrons in the metal. When $\omega^2+\nu^2<\omega_p^2$ (which is the case for many metals at optical wavelengths) a negative value for the real part $\epsilon_{r,2}$ is obtained, implying that plasmon-polariton modes can be supported at interfaces with normal dielectrics.

B. Electromagnetic wave and field equations

The modes supported by the structure illustrated in Fig. 1 are obtained by solving a suitably defined boundary value problem based on Maxwell's equations written in the frequency domain for a lossy inhomogeneous isotropic medium. Uncoupling Maxwell's equations yields the following time-harmonic vectorial wave equations for the **E** and **H** fields:

$$\nabla\times\nabla\times\mathbf{E}-\omega^2\epsilon(x,y)\mu\mathbf{E}=0, \tag{2}$$

$$\nabla\times\epsilon(x,y)^{-1}\nabla\times\mathbf{H}-\omega^2\mu\mathbf{H}=0, \tag{3}$$

where the permittivity ϵ is a complex function of cross-sectional space, and describes the wave guide structure. For the structures analyzed in this paper, μ is homogeneous and taken as the permeability of free space μ_0.

Due to the nature of the numerical method used to solve the boundary value problem, the implicit y dependence of the permittivity can be immediately removed since any inhomogeneity along y is treated by dividing the structure into a number of layers that are homogeneous along this direction, and suitable boundary conditions are applied between them.

The two vectorial wave equations (2) and (3) are expanded in each layer into scalar wave equations, some being coupled by virtue of the remaining inhomogeneity in ϵ along x. Since the structure under consideration is invariant along the propagation axis (taken to be in the $+z$ direction), the mode fields vary along this dimension according to $e^{-\gamma z}$ where $\gamma=\alpha+j\beta$ is the complex propagation constant of the mode, α is the attenuation constant, and β is the phase constant. Substituting this field dependency into the scalar wave equations, and writing them for TE^x ($E_x=0$) and TM^x ($H_x=0$) modes while making use of $\nabla\cdot[\epsilon(x)\mathbf{E}]=0$ and $\nabla\cdot\mathbf{H}=0$ accordingly, yields simplified and uncoupled scalar wave equations that are readily solved. The E_y component of the TE^x modes must satisfy the Helmholtz wave equation

$$\frac{\partial^2}{\partial x^2}E_y^{TE}+\frac{\partial^2}{\partial y^2}E_y^{TE}+[\gamma^2+\omega^2\mu\epsilon(x)]E_y^{TE}=0 \tag{4}$$

and the H_y component of the TM^x modes must satisfy the Sturm-Liouville wave equation

$$\epsilon(x)\frac{\partial}{\partial x}\left[\frac{1}{\epsilon(x)}\frac{\partial}{\partial x}H_y^{TM}\right]+\frac{\partial^2}{\partial y^2}H_y^{TM}+[\gamma^2+\omega^2\mu\epsilon(x)]H_y^{TM}=0. \tag{5}$$

The superposition of the TE^x and TM^x mode families then describes any mode propagating in the structure analyzed. The electric and magnetic field components resulting from this superposition are given by the following equations:

$$E_x=\frac{-1}{j\omega\gamma}\left[\frac{\partial}{\partial x}\left(\frac{1}{\epsilon(x)}\frac{\partial}{\partial x}H_y^{TM}\right)+\omega^2\mu H_y^{TM}\right], \tag{6}$$

$$E_y=E_y^{TE}-\frac{1}{j\omega\gamma\epsilon(x)}\frac{\partial^2}{\partial x\partial y}H_y^{TM}, \tag{7}$$

$$E_z=\frac{1}{\gamma}\frac{\partial}{\partial y}E_y^{TE}+\frac{1}{j\omega\epsilon(x)}\frac{\partial}{\partial x}H_y^{TM}, \tag{8}$$

$$H_x=\frac{1}{j\omega\gamma}\left[\frac{1}{\mu}\frac{\partial^2}{\partial x^2}E_y^{TE}+\omega^2\epsilon(x)E_y^{TE}\right], \tag{9}$$

$$H_y=\frac{1}{j\omega\gamma\mu}\frac{\partial^2}{\partial x\partial y}E_y^{TE}+H_y^{TM}, \tag{10}$$

$$H_z=\frac{-1}{j\omega\mu}\frac{\partial}{\partial x}E_y^{TE}+\frac{1}{\gamma}\frac{\partial}{\partial y}H_y^{TM}. \tag{11}$$

In order to obtain a mode of propagation supported by a wave guiding structure, the Helmholtz and Sturm-Liouville wave equations (4) and (5), along with the field equations (6)–(11), must be solved for the propagation constant γ using appropriate boundary conditions applied between layers and at the horizontal and vertical limits.

C. Poynting vector and power confinement factor

The power confinement factor is defined as the ratio of mode complex power carried through a portion of a wave guide's cross section with respect to the mode complex power carried through the entire wave guide cross section. Formally it is expressed as

$$cf=\frac{|\int\int_{A_c}S_z ds|}{|\int\int_{A_\infty}S_z ds|}, \tag{12}$$

where A_c is usually taken as the area of the wave guide core and A_∞ implies integration over the entire wave guide cross section (which can be all cross-sectional space for an open structure) or the entire cross-sectional computational domain. S_z refers to the z component of the Poynting vector

$$S_z=\frac{1}{2}(E_xH_y^*-E_yH_x^*) \tag{13}$$

and $H_{x,y}^*$ denotes the complex conjugate of $H_{x,y}$. The spatial distribution of a component of the Poynting vector is easily computed from the spatial distribution of the relevant electric and magnetic mode field components.

D. Numerical solution approach

The boundary value problem governed by equations (4)–(11) is solved by applying the method of lines (MoL). The MoL is a well-known numerical technique and its application to various electromagnetic problems, including optical wave guiding, is well established.[14] The MoL is rigorous, accurate, and flexible. It can handle a wide variety of wave guide geometries, including the structures at hand. The method is not known to generate spurious or nonphysical modes.

The MoL formulation used in this study is based on the formulation reported in Ref. 15, but simplified for isotropic media, as prescribed by Eqs. (4)–(11) and reported in Ref. 16. Except for a 1D spatial discretization, the method is exact.

The main idea behind the MoL is that the differential field equations governing a wave guiding problem are discretized only as far as necessary so that generalized analytic solutions can be applied to derive a homogeneous matrix problem describing all modes supported by the structure. This approach renders the method accurate and computationally efficient since only N-1 dimensions must be discretized to solve an N dimension problem. In the case of a 2D wave guiding structure, this means that only one spatial dimension needs to be discretized. The main features of this procedure, as applied to a modal analysis problem are described below.

The x axis and the function $\epsilon(x)$ are discretized using two shifted nonequidistant line systems, parallel to the y axis.

The differential operators $\partial/\partial x$ and $\partial^2/\partial x^2$ in the wave and field equations are replaced by finite difference approximations that include the lateral boundary conditions.

The discretized wave equations are diagonalized using appropriate transformations matrices.

The diagonalization procedure yields in the transform domain two systems of uncoupled 1D differential equations along the remaining dimension (in this case along the y axis).

These differential equations are solved analytically and tangential field matching conditions are applied at interfaces between layers along with the top and bottom boundary conditions.

The last field matching condition, applied near the center of the structure, yields a homogeneous matrix equation of the form $G(\gamma)\tilde{e}=0$ which operates on transformed tangential fields.

The complex propagation constant γ of modes is then obtained by searching for values that satisfy $\det[G(\gamma)]=0$.

Once the propagation constant of a mode has been determined, the spatial distribution of all six field components of the mode are easily generated.

A mode power confinement factor can be computed by first computing the spatial distribution of S_z which is then integrated according to Eq. (12).

The open structure shown in Fig. 1 is discretized along the x axis and the generalized analytic solution applied along the y axis. The physical symmetry of the structure is exploited to increase the accuracy of the results and to reduce the numerical effort required to generate the mode solutions. This is achieved by placing either electric wall ($E_{\tan}=0$) or magnetic wall ($H_{\tan}=0$) boundary conditions along the x and y axes. The remaining top boundary condition is placed at infinity and the remaining lateral boundary condition is either placed far enough from the guide to have a negligible effect on the mode calculation, or a lateral absorbing boundary condition is used to simulate infinite space, depending on the level of confinement observed in the resulting mode.

The use of numerical methods to solve differential equations inevitably raises questions regarding the convergence

of computed results and their accuracy. The propagation constant of a mode computed using the method of lines converges in a monotonic or smooth manner with a reduction in the discretization interval (which increases the number of lines in the calculation and thus the numerical effort). This suggests that extrapolation can be used to generate a more accurate value for the propagation constant, and this value can then be used to compute the error in values obtained using the coarser discretizations.[17] This *anticipated error* does not correspond to the actual error in the propagation constant as the latter could only be known if the analytic or exact value is available. The anticipated error however still provides a useful measure of accuracy since it must tend toward zero as more accurate results are generated.

The convergence of the computed propagation constant of the modes supported by the structures of interest has been monitored during the entire study. The anticipated error in the results presented in this paper is estimated as 1% on average and 6% in the worst case. These error values are based on extrapolated propagation constants computed using Richardson's extrapolation formula.[18]

III. MODE CHARACTERISTICS AND EVOLUTION WITH FILM THICKNESS

A. Review of mode solutions for metal film slab wave guides

The study begins with the reproduction of results for an infinitely wide symmetric metal film wave guide, as shown in Fig. 1 with $w=\infty$, taken from the standard work on such structures.[6] In order to remain consistent with their results, the optical free-space wavelength of excitation is set to $\lambda_0 = 0.633\,\mu$m and their value for the relative permittivity of the silver film at this wavelength is used: $\epsilon_{r,2} = -19 - j0.53$. The relative permittivity of the top and bottom dielectric regions is set to $\epsilon_{r,1}=4$.

An infinitely wide structure supports only two purely bound TM ($E_x=H_y=H_z=0$) modes having transverse field components E_y and H_x that exhibit asymmetry or symmetry with respect to the x axis. These modes are created from the coupling of individual plasmon-polariton modes supported by the top and bottom interfaces and they exhibit dispersion with film thickness. The widely accepted nomenclature for identifying them consists in using the letters a or s for asymmetric or symmetric transverse field distributions, respectively, followed by a subscript b or l for bound or leaky modes, respectively. The propagation constants of the a_b and s_b modes have been computed as a function of film thickness and the normalized phase and attenuation constants are plotted in Figs. 2(a) and 2(b), respectively.

From Fig. 2, it is observed that the a_b and s_b modes become degenerate with increasing film thickness. As the separation between the top and bottom interfaces increases, the a_b and s_b modes begin to split into a pair of uncoupled plasmon-polariton modes localized at the metal-dielectric interfaces. The propagation constants of the a_b and s_b modes thus tend towards that of a plasmon-polariton mode supported by the interface between semi-infinite metallic and dielectric regions, which is given via the following equations:[6]

$$\beta/\beta_0 = \mathrm{Re}\left\{ \sqrt{\frac{\epsilon_{r,1}\epsilon_{r,2}}{\epsilon_{r,1}+\epsilon_{r,2}}} \right\}, \tag{14}$$

$$\alpha/\beta_0 = -\mathrm{Im}\left\{ \sqrt{\frac{\epsilon_{r,1}\epsilon_{r,2}}{\epsilon_{r,1}+\epsilon_{r,2}}} \right\}, \tag{15}$$

where $\beta_0=\omega/c_0$ with c_0 being the velocity of light in free space, and $\epsilon_{r,1}$ and $\epsilon_{r,2}$ are the complex relative permittivities of the materials used. Using the above equations, values of $\beta/\beta_0=2.250646$ and $\alpha/\beta_0=0.836247\times10^{-2}$ are obtained for $\epsilon_{r,1}=4$ and $\epsilon_{r,2}=-19-j0.53$.

As the thickness of the film decreases, the phase and attenuation constants of the a_b mode increase, becoming very large for very thin films. This is due to the fact that the fields of this mode penetrate progressively deeper into the metal as its thickness is reduced. In the case of the s_b mode, a decreasing film thickness causes the opposite effect, that is, the fields penetrate progressively more into the top and bottom dielectric regions and less into the metal. The propagation constant of this mode thus tends asymptotically towards that of a transverse electromagnetic (TEM) wave propagating in an infinite medium having the same permittivity as the top and bottom dielectric regions. In this case, the attenuation constant decreases asymptotically towards zero since losses were neglected in these regions. The a_b and s_b modes do not have a cutoff thickness.

The fields in an infinitely wide structure do not exhibit any spatial variation along x. Due to the nature of the MoL, and to the fact that the generalized analytical solution is applied along the y dimension, our results do not contain discretization errors and thus are in perfect agreement with those reported in Ref. 6.

B. Modes supported by a metal film of width $w=1\,\mu$m

The study proceeds with the analysis of the structure shown in Fig. 1 for the case $w=1\,\mu$m. The material parameters and free-space wavelength that were used in the previous case ($w=\infty$) were also used here. The MoL was applied and the discretization adjusted until convergence of the propagation constant was observed. The physical quarter symmetry of the structure was exploited by placing vertical and horizontal electric or magnetic walls along the y and x axes, respectively, which leads to four possible wall combinations as listed in Table I. The first two purely bound (nonleaky) modes for each wall combination was found and their dispersion with metal thickness computed. The results for these eight modes are shown in Fig. 2.

Unlike its slab counterpart, pure TM modes are not supported by a metal film of finite width: all six field components are present in all modes. For a symmetric structure having an aspect ratio $w/t>1$, the E_y field component dominates. The E_x field component increases in magnitude with increasing film thickness and if $w/t<1$, then E_x dominates. Recently, a proposal was made to identify the modes supported by a metal film of finite width, by extending the nomenclature used for metal film slab wave guides.[13] First a pair of letters being a or s identify whether the main transverse electric field component is asymmetric or symmetric with respect to the y and x axes, respectively (in most practical structures $w/t\gg1$ and E_y is the main transverse electric

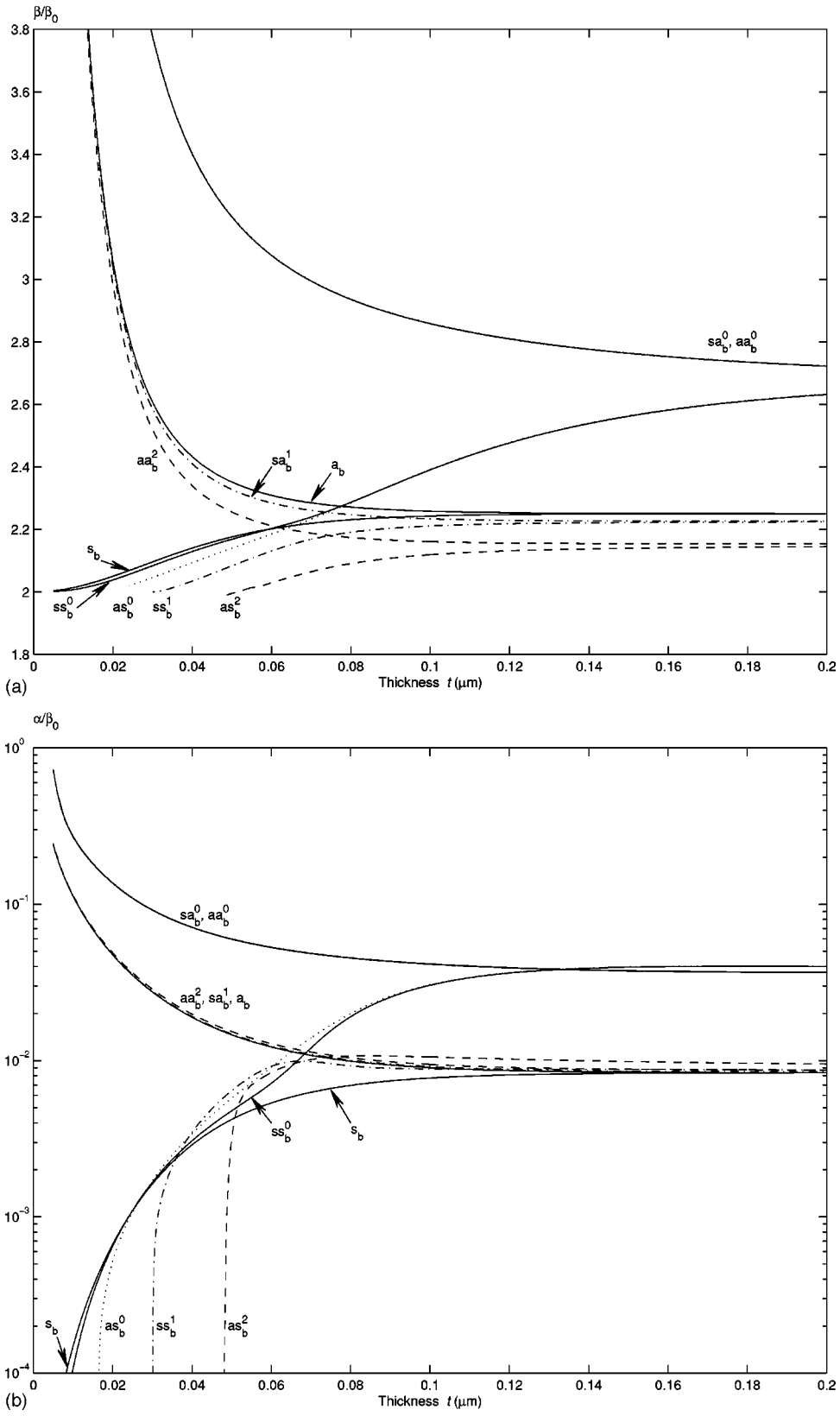

FIG. 2. Dispersion characteristics with thickness of the first eight modes supported by a metal film wave guide of width $w=1$ μm. The a_b and s_b modes supported for the case $w=\infty$ are shown for comparison. (a) Normalized phase constant. (b) Normalized attenuation constant.

field component). A superscript is then used to track the number of extrema observed in the spatial distribution of this field component along the largest dimension (usually along the x axis) between the corners. A second superscript n could be added to track the extrema along the other dimension (the y axis) if modes exhibiting them are found. Finally, a sub-

TABLE I. Vertical-horizontal wall combinations used along the axes of symmetry and proposed mode nomenclature. ew: electric wall, mw: magnetic wall.

V-H walls	Mode
ew-ew	as_b^m
mw-ew	ss_b^m
mw-mw	sa_b^m
ew-mw	aa_b^m

script *b* or *l* is used to identify whether the mode is bound or leaky. Leaky modes are known to exist in metal film slab structures and though they have not been characterized in the present study, their existence is anticipated. Table I relates the proposed mode nomenclature to the corresponding vertical and horizontal wall combinations used along the axes of symmetry.

The ss_b^0, sa_b^0, as_b^0, and aa_b^0 modes are the first modes generated (one for each of the four possible quarter-symmetries listed in Table I, and having the largest phase constant) and thus may be considered as the fundamental modes supported by the structure. Figures 3–6 show the field distributions of these modes over the cross section of the wave guide for a metal film of thickness $t=100$ nm. As is observed from these figures, the main transverse electric field component is the E_y component and the symmetries in the spatial distribution of this component are reflected in the mode nomenclature. The outline of the metal is clearly seen in the distribution of the E_y component on all of these plots. As is observed from the figures, very little field couples par-

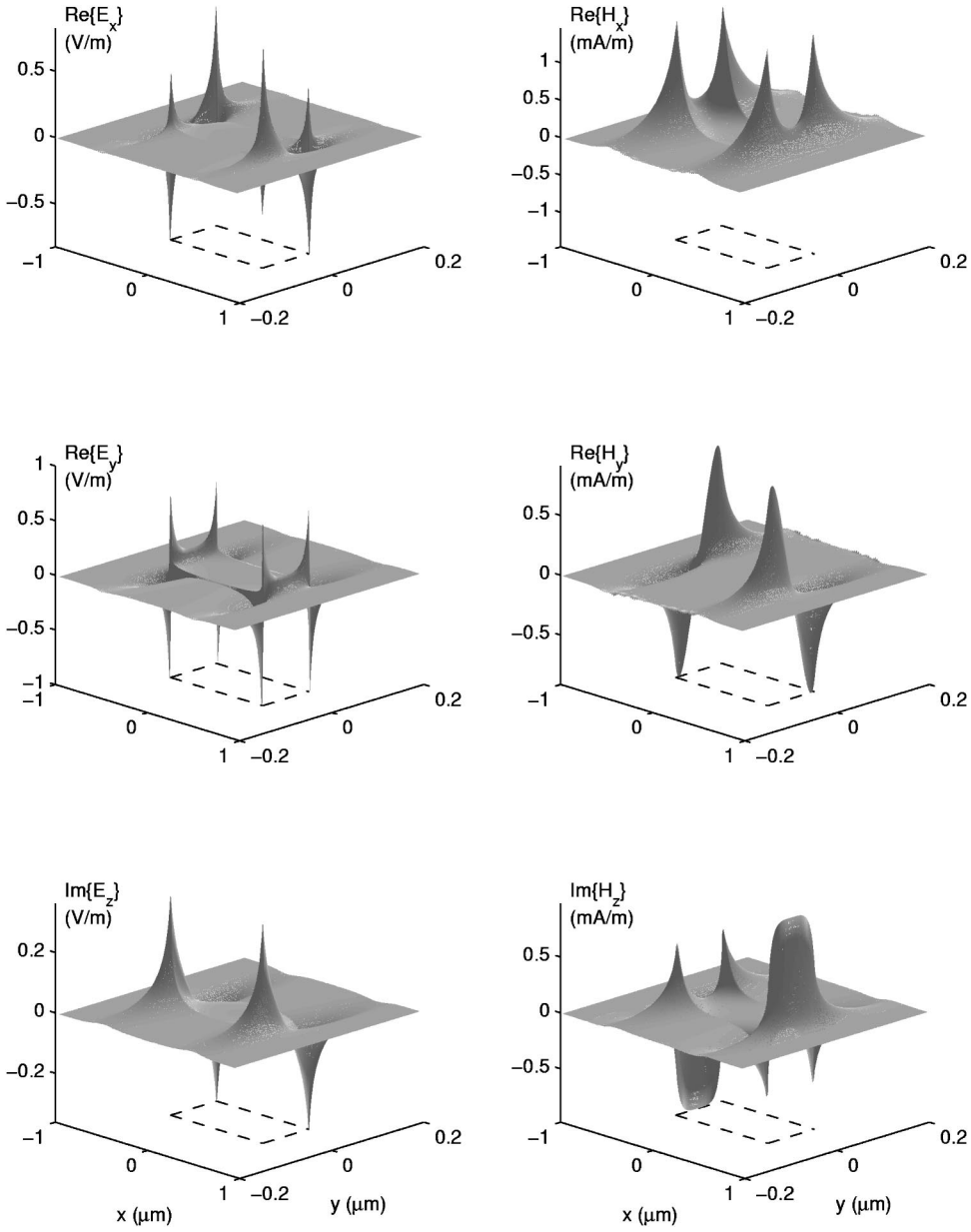

FIG. 3. Spatial distribution of the six field components related to the ss_b^0 mode supported by a metal film wave guide of thickness $t=100$ nm and width $w=1$ μm. The waveguide cross section is located in the *x-y* plane and the metal is bounded by the region $-0.5 \leqslant x \leqslant 0.5$ μm and $-0.05 \leqslant y \leqslant 0.05$ μm, outlined as the rectangular dashed contour. The field distributions are normalized such that $\max|\mathrm{Re}\{E_y\}|=1$.

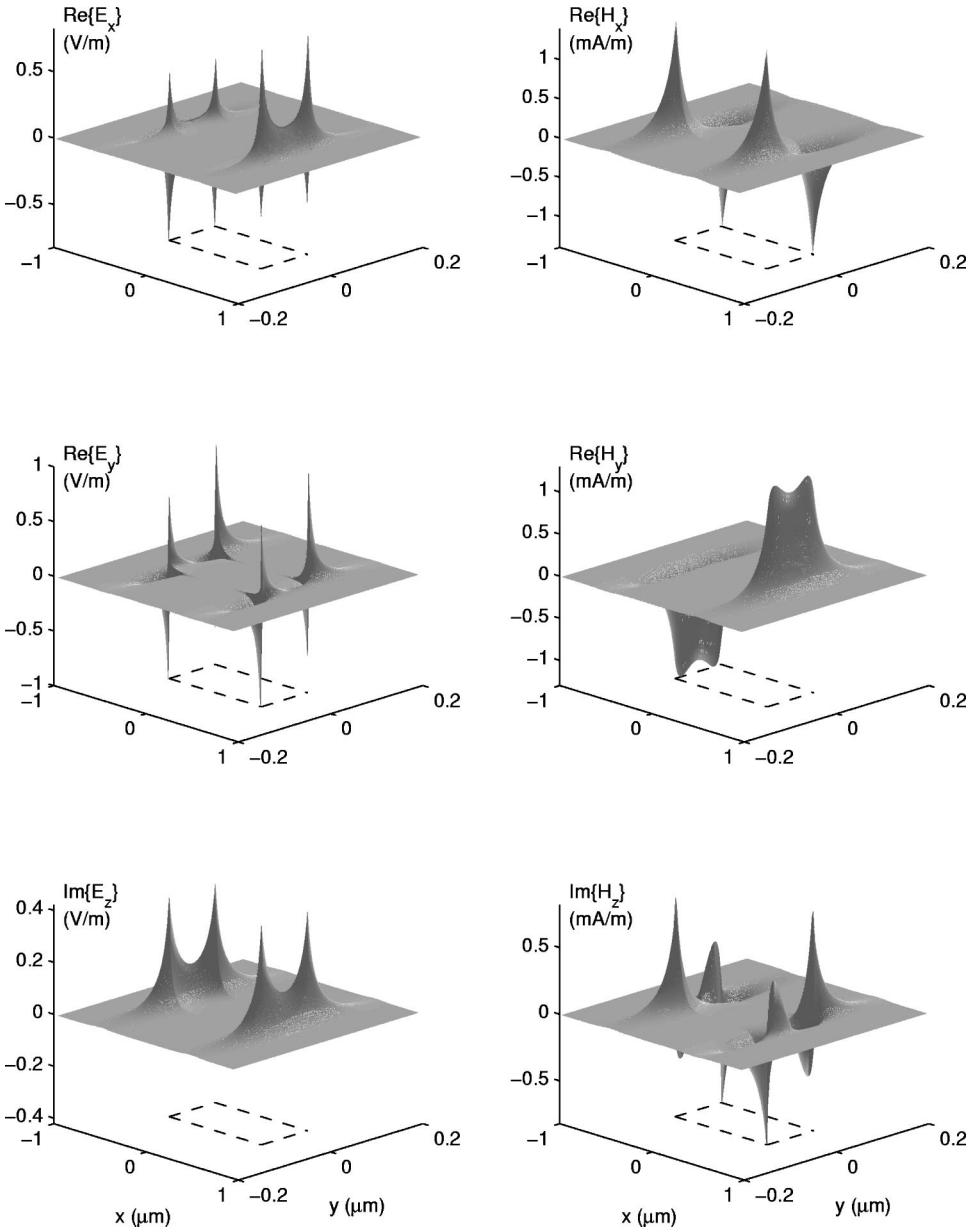

FIG. 4. Spatial distribution of the six field components related to the sa_b^0 mode supported by a metal film wave guide of thickness $t=100\,\mathrm{nm}$ and width $w=1\,\mu\mathrm{m}$. The wave guide cross section is located in the x-y plane and the metal is bounded by the region $-0.5\leqslant x\leqslant 0.5\,\mu\mathrm{m}$ and $-0.05\leqslant y\leqslant 0.05\,\mu\mathrm{m}$, outlined as the rectangular dashed contour. The field distributions are normalized such that $\max|\mathrm{Re}\{E_y\}|=1$.

allel edges for this case of film thickness and width (very little coupling through the metal between the top and bottom edges and between the left and right edges), though coupling does occur along all edges between adjacent corners (mostly along the left and right ones), and also between perpendicular edges through the corner.

Figure 2 suggests that the dispersion curves for these first four modes converge with increasing film thickness toward the propagation constant of a plasmon-polariton mode supported by an isolated corner (though pairs of corners in this case remain weakly coupled along the top and bottom edges due to the finite width of the film, even if its thickness goes to infinity). If both the film thickness and width were to increase further, the four fundamental modes would approach degeneracy with their propagation constants tending towards that of a plasmon-polariton mode supported by an isolated corner, and their mode fields becoming more localized near the corners of the structure with maxima occuring at all four corners and fields decaying in an exponential-like manner in all directions away from the corners. This is further supported by considering the evolution of the field distributions given in Figs. 3 to 6 as both the thickness and width increase.

As the thickness of the film decreases, coupling between the top and bottom edges increases and the four modes split into a pair as the upper branch (modes sa_b^0 and aa_b^0 which have a dominant E_y field component exhibiting asymmetry with respect to the x axis) and a pair as the lower branch (modes ss_b^0 and as_b^0 which have a dominant E_y field component exhibiting symmetry with respect to the x axis), as shown in Fig. 2. The pair on the upper branch remain approximately degenerate for all film thicknesses, though decreasing the film width would eventually break this degeneracy. The upper branch modes do not change in character as the film thickness decreases. Their field distributions remain essentially unchanged from those shown in Figs. 4 and 6 with the exception that confinement to the metal region is increased thus causing an increase in their attenuation constant. This field behavior is consistent with that of the a_b mode supported by a metal film slab wave guide.

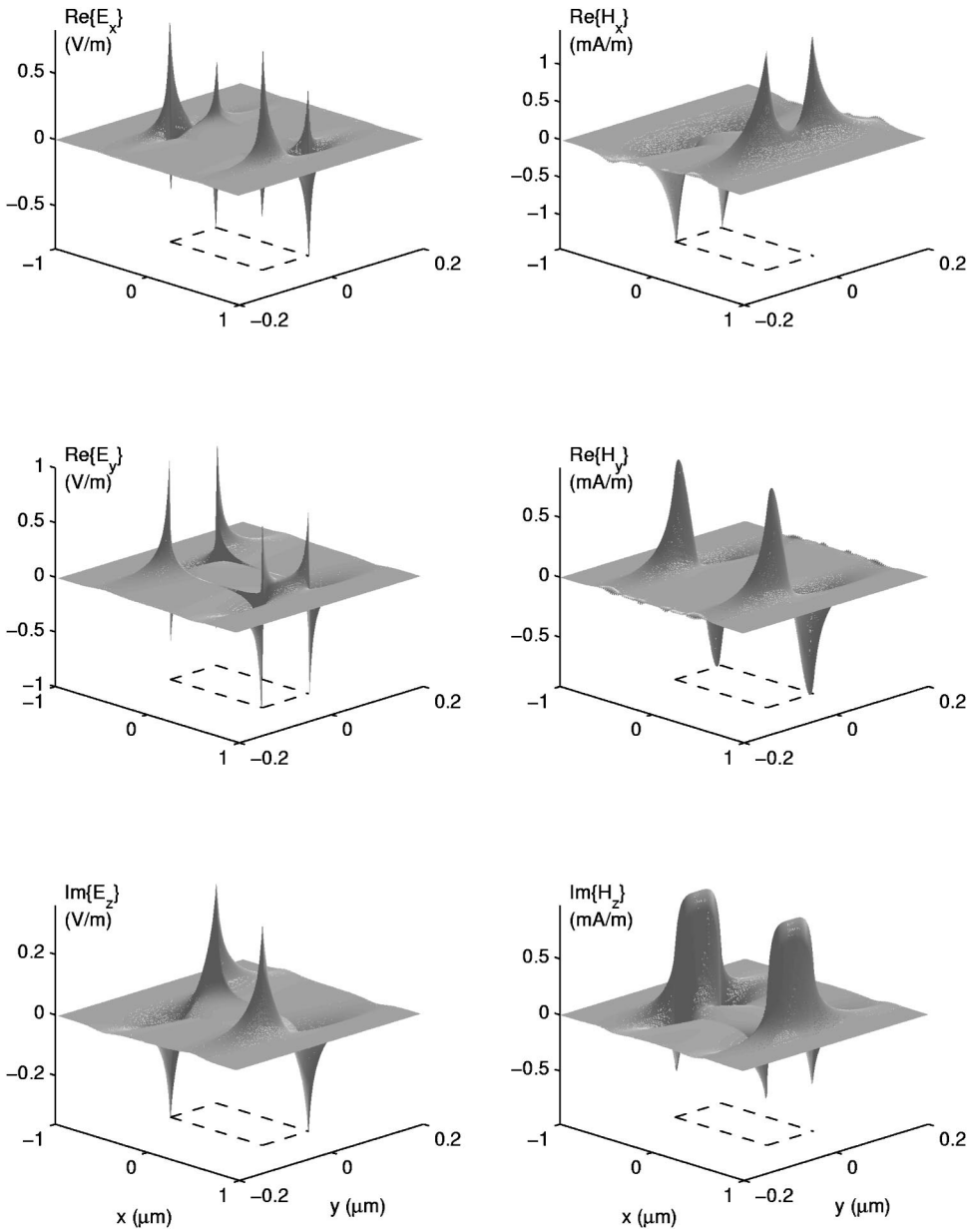

FIG. 5. Spatial distribution of the six field components related to the as_b^0 mode supported by a metal film wave guide of thickness $t = 100$ nm and width $w = 1$ μm. The waveguide cross section is located in the x-y plane and the metal is bounded by the region $-0.5 \leqslant x \leqslant 0.5$ μm and $-0.05 \leqslant y \leqslant 0.05$ μm, outlined as the rectangular dashed contour. The field distributions are normalized such that the $\max|\mathrm{Re}\{E_y\}| = 1$.

The modes on the lower branch begin to split at a film thickness of about 80 nm, as shown in Fig. 2. As the film thickness decreases further the ss_b^0 mode follows closely the phase and attenuation curves of the s_b mode supported by the metal film slab wave guide. In addition to exhibiting dispersion, the lower branch modes change in character with decreasing thickness, their field evolving from being concentrated near the corners, to having Gaussian-like distributions along the wave guide width. The E_y field component of the ss_b^0 mode develops an extremum near the center of the top and bottom interfaces, while that of the as_b^0 mode develops two extrema, one on either side of the center. Since these modes change in character, they should be identified when the film is fairly thick.

Figure 7 shows the evolution of the ss_b^0 mode fields with film thickness via contour plots of $\mathrm{Re}\{S_z\}$. S_z is computed from the ss_b^0 modes fields using Eq. (13) and corresponds to the complex power density carried by the mode. The power confinement factor cf is also given in the figure for all cases, and is computed via Eq. (12) with the area of the wave guide core A_c taken as the area of the metal region. Figure 7 clearly shows how the mode fields evolve from being confined to the corners of thick films to being distributed in a Gaussian-like manner laterally along the top and bottom edges, as the field coupling between these edges increases due to a reduction in film thickness. The confinement factor becomes smaller as the film thickness decreases, ranging from 14% confinement to 1.6% as the thickness goes from 80 to 20 nm. This implies that fields become less confined to the metal, spreading out not only along the vertical dimension but along the horizontal one as well, as is observed by comparing parts (a) and (f) of Fig. 7. This reduction in confinement to the

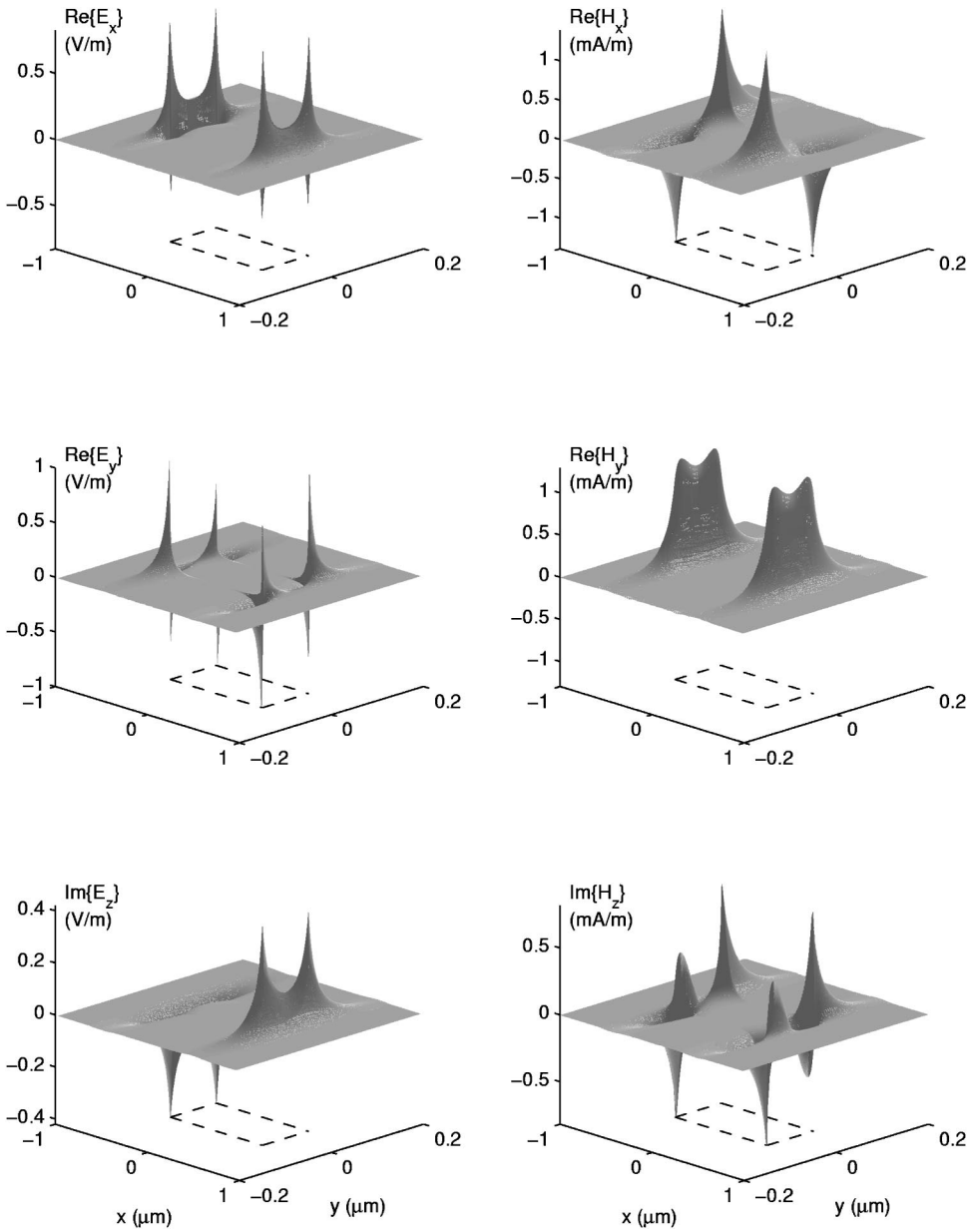

FIG. 6. Spatial distribution of the six field components related to the aa_b^0 mode supported by a metal film wave guide of thickness $t=100$ nm and width $w=1$ μm. The waveguide cross section is located in the x-y plane and the metal is bounded by the region $-0.5\leqslant x\leqslant 0.5$ μm and $-0.05\leqslant y\leqslant 0.05$ μm, outlined as the rectangular dashed contour. The field distributions are normalized such that $\max|\mathrm{Re}\{E_y\}|=1$.

lossy metal region, explains the reduction in the attenuation constant of the mode with decreasing film thickness, as shown in Fig. 2(b). An examination of all field components related to the ss_b^0 mode reveals that the magnitude of the weak transverse (E_x,H_y) and longitudinal (E_z,H_z) components decrease with decreasing film thickness implying that the mode is evolving towards a TEM mode comprised of the E_y and H_x field components. Indeed, the normalized propagation constant of the ss_b^0 mode tends asymptotically towards the value of the normalized propagation constant of a TEM wave propagating in the background material ($\epsilon_{r,1}=4$ with no losses in this case), further supporting this fact. This field behavior is also consistent with that of the s_b mode supported by a metal film slab wave guide.

Figure 8 shows the profile of $\mathrm{Re}\{S_z\}$ of the ss_b^0 mode over the cross section of the guide for the case $t=20$ nm, providing a different perspective of the same information plotted as contours in Fig. 7(f). Figure 8 shows that $\mathrm{Re}\{S_z\}$ is negative in the metal film, implying that the mode real power is flowing in the direction opposite to the direction of mode propagation (or to the direction of phase velocity) in this region. It is clear, however, that the overall or net mode real power is flowing along the direction of propagation. It is likely that the net mode real power can be made to flow in the direction opposite to that of phase velocity (as in metal film slab wave guides[10]) for values of $\epsilon_{r,1}$ in the neighborhood or greater than $|\mathrm{Re}\{\epsilon_{r,2}\}|$.

Unlike the metal film slab waveguide, a metal film of finite width can support a number of higher order modes. The dispersion curves of the first four higher order modes (each generated from one of the symmetries listed in Table I) are shown in Fig. 2, and the spatial distribution of their main

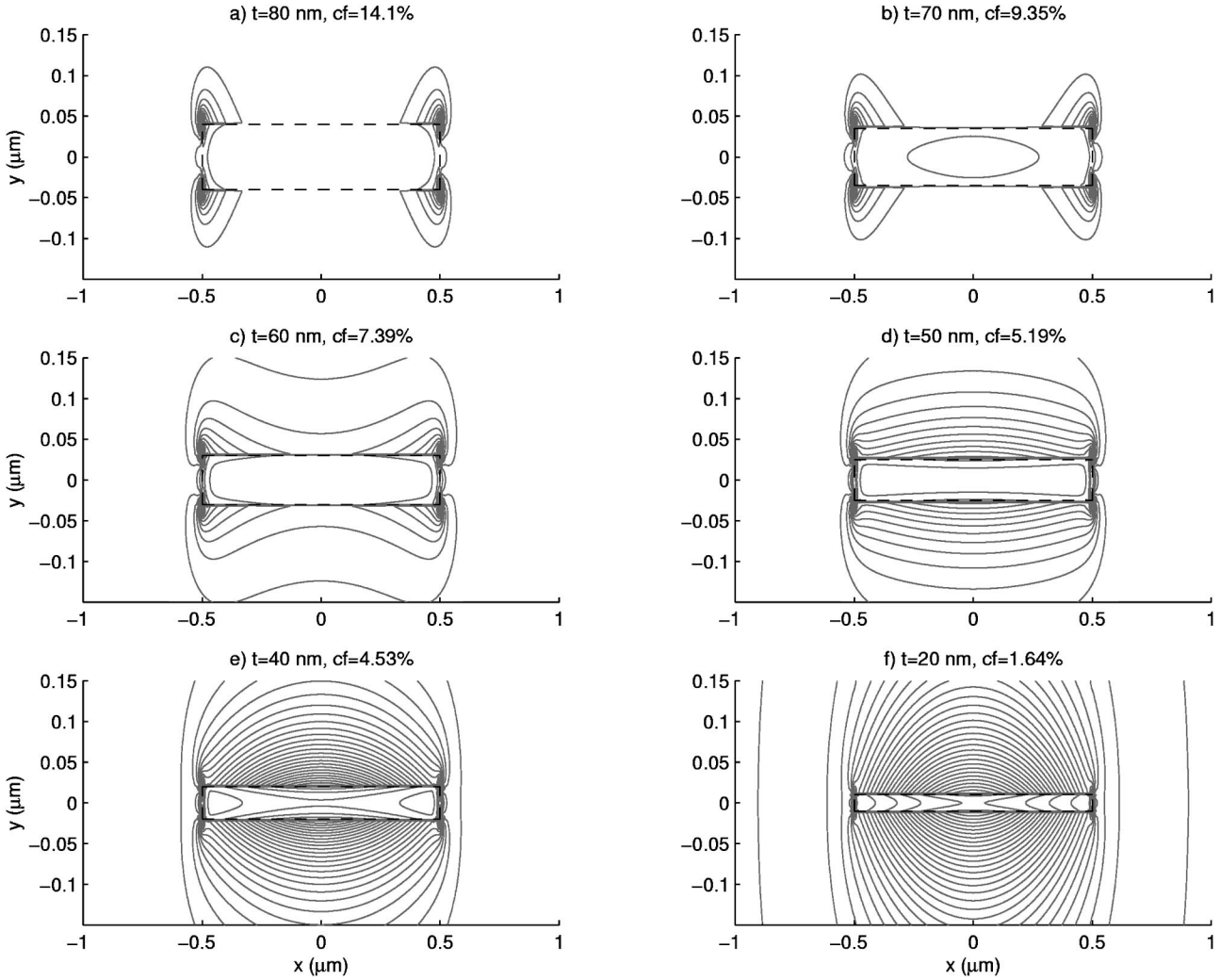

FIG. 7. Contour plot of Re$\{S_z\}$ associated with the ss_b^0 mode for metal film wave guides of width $w=1$ μm and various thicknesses. The power confinement factor cf is also given in all cases, and is computed via Eq. (12) with the area of the wave guide core A_c taken as the area of the metal region. In all cases, the outline of the metal film is shown as the rectangular dashed contour.

transverse electric field component is shown in Fig. 9 for a film of thickness $t=100$ nm. As is observed from Fig. 9, the symmetries and number of extrema in the distributions of Re$\{E_y\}$ are reflected in the mode nomenclature. It should be noted that the nature of the nomenclature is such that all higher order modes sa_b^m and ss_b^m have an odd m while all higher order modes aa_b^m and as_b^m have an even m. Comparing parts (a)–(d) of Fig. 9 with the E_y field component of the corresponding $m=0$ mode in Figs. 3–6 [i.e., comparing the E_y component of the ss_b^1 mode shown in Fig. 9(a) with the E_y component of the ss_b^0 mode shown in Fig. 3, etc.] reveals that the fields of a higher order mode are comprised of the fields of the corresponding $m=0$ mode with additional spatial oscillations or variations along the top and bottom edges of the structure due to the latter's limited width. Making this comparison for all of the field components of the higher order modes found reveals this fact to be true, except for the H_y field component which remains in all cases essentially identical to that of the corresponding $m=0$ mode; ie: the H_y field component never exhibits oscillations along the width of the structure.

The evolution of the sa_b^1 and aa_b^2 modes with film thickness is similar to the evolution of the sa_b^0 and aa_b^0 modes (and the a_b mode supported by the metal film slab wave guide), in that their mode fields become more tightly confined to the metal as the thickness of the latter decreases, thereby causing an increase in the attenuation of the modes, as shown in Fig. 2(b). Furthermore, the sa_b^1 and aa_b^2 modes do not change in character with film thickness, their field distributions remaining essentially unchanged in appearance from those computed at a thickness of 100 nm.

The ss_b^1 and as_b^2 modes evolve with thickness in a manner similar to the corresponding $m=0$ modes (and the s_b mode of the metal film slab wave guide) in the sense that their fields become less confined to the metal region as the thickness of the latter decreases, thereby reducing the attenuation of the modes as shown in Fig. 2(b). As the thickness of the film decreases, the ss_b^1 and as_b^2 modes change in character in a manner similar to the corresponding $m=0$ modes, their field components evolving extra variations along the top and bottom edges.

As the thickness of the film increases, the propagation constants of the sa_b^1 and ss_b^1 modes converge to a single complex value as shown in Fig. 2. This is the propagation constant of uncoupled higher order modes supported by the

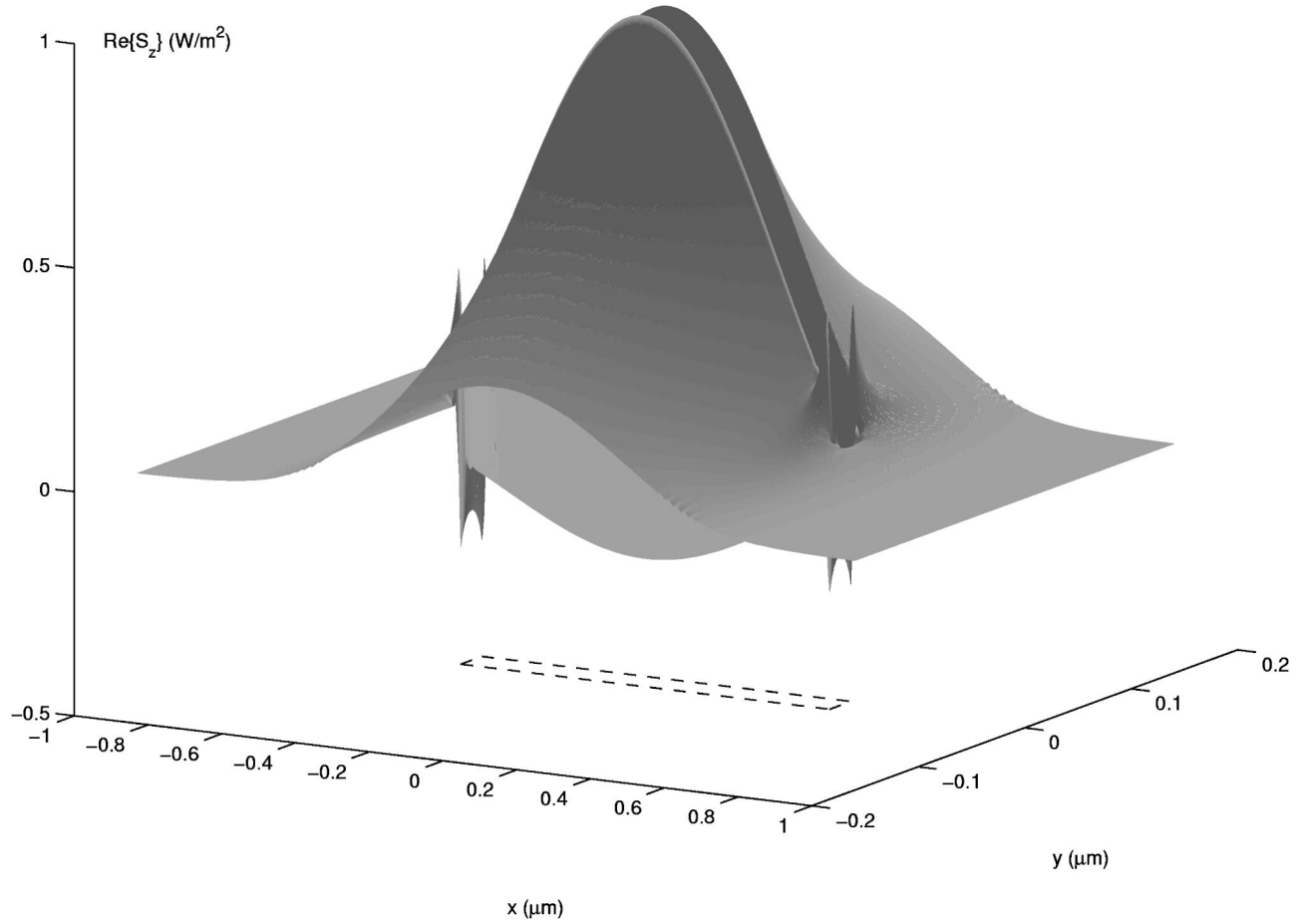

FIG. 8. Normalized profile of $\mathrm{Re}\{S_z\}$ associated with the ss_b^0 mode for a metal film wave guide of width $w=1\ \mu$m and thickness $t=20$ nm. The wave guide cross section is located in the x-y plane and the metal film is bounded by the region $-0.5\leqslant x\leqslant 0.5\ \mu$m and $-0.01\leqslant y\leqslant 0.01\ \mu$m, outlined as the rectangular dashed contour.

top and bottom edges of the film. A similar observation holds for the aa_b^2 and as_b^2 modes. The nature of these ''edge modes'' is clear by considering the evolution with increasing film thickness of the distributions shown in Fig. 9. As the thickness of the film tends to infinity, the top edge becomes uncoupled from the bottom edge, forcing the ss_b^1 mode to become degenerate with the sa_b^1 mode since both have an E_y field component that is symmetric with respect to the y axis and one extremum in its distribution along the top or bottom edge. A similar reasoning explains why the as_b^2 mode must become degenerate with the ss_b^2 mode. In general, it is expected that the higher order sa_b^m and ss_b^m mode families will form degenerate pairs for a given m, as will the higher order as_b^m and aa_b^m mode families, with increasing film thickness.

The aa_b^m and sa_b^m mode families do not have mode cutoff thickness. This is due to the fact that their confinement to the metal film increases with decreasing film thickness, thus the modes remain guided as $t\rightarrow 0$. The as_b^m and ss_b^m mode families have cutoff thickness for all modes except the ss_b^0 mode, which remains guided at $t\rightarrow 0$, since it evolves into the TEM mode supported by the background. The other modes of these families, including the as_b^0 mode cannot propagate as $t\rightarrow 0$ because their mode fields do not evolve into a TEM mode. Rather, the modes maintain extrema in their field distributions and such variations cannot be supported by an infinite homogeneous medium.

In general, the purely bound modes supported by a metal film of finite width appear to be formed from a coupling of modes supported by each metal-dielectric interface defining the structure. In a metal film of finite width, straight interfaces of finite length (top, bottom, left, and right edges) and corner interfaces are present. Since a straight metal-dielectric interface of infinite length can support a bound plasmon-polariton mode then so should an isolated corner interface and a straight interface of finite length bounded by corners (say the edge defined by a metal of finite width having an infinite thickness). A preliminary analysis of an isolated corner has revealed that a plasmon-polariton mode is indeed supported and that the phase and attenuation constants of this mode are greater than those of the mode guided by the corresponding infinite straight interface, as given by Eqs. (14) and (15). This is due to the fact that fields penetrate more deeply into the metal near the corner, to couple neighboring perpendicular edges. All six field components are present in such a mode, having their maximum value at the corner and decreasing in an exponential-like manner in all directions away from the corner. A straight interface of finite length bounded by corners should support a discrete spectrum of plasmon-polariton modes with the defining feature in the mode fields being the number of extrema in their spatial distribution along the edge. A mode supported by a metal film of finite width may therefore be seen as being comprised of coupled ''corner modes'' and ''finite length edge modes.''

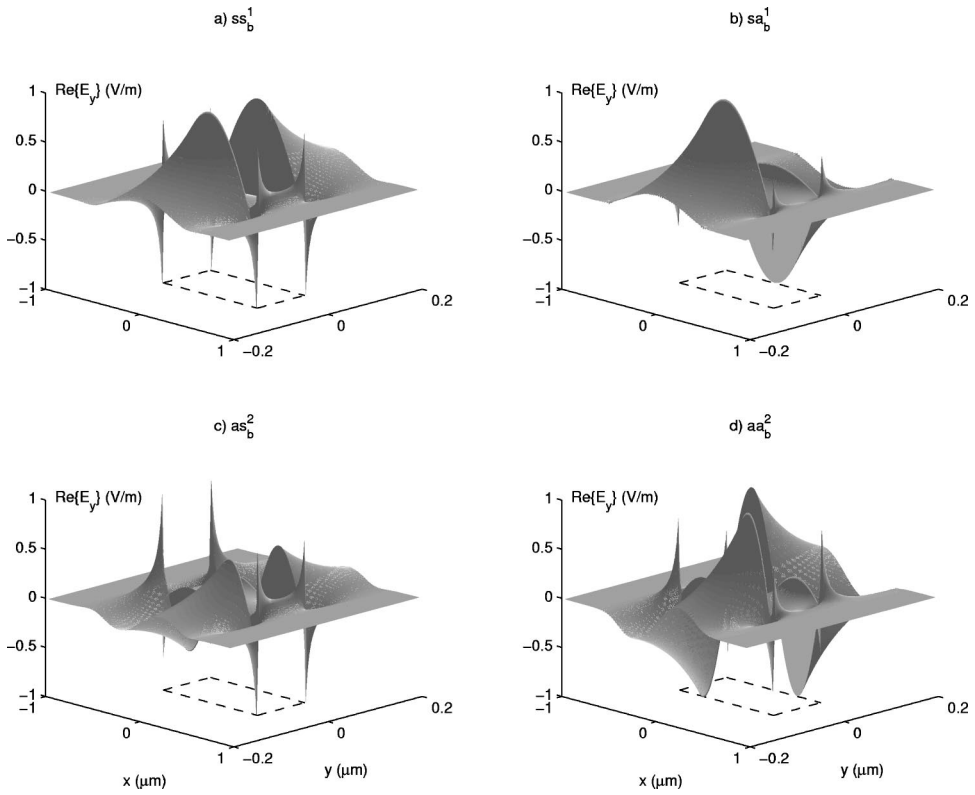

FIG. 9. Spatial distribution of the E_y field component related to some higher order modes supported by a metal film wave guide of thickness $t=100$ nm and width $w=1$ μm. In all cases, the wave guide cross section is located in the x-y plane and the metal film is bounded by the region $-0.5 \leqslant x \leqslant 0.5$ μm and $-0.05 \leqslant y \leqslant 0.05$ μm, outlined as the rectangular dashed contour.

The ss_b^0 mode could be used for optical signal transmission over short distances. Its losses decrease with decreasing film thickness in a manner similar to the s_b mode supported by the metal film slab wave guide. In a symmetric structure such as the one studied here, the ss_b^0 mode does not have a cutoff thickness thus losses could be made small enough to render it long ranging, though a trade off against confinement is necessary. In addition, when the metal is thin the E_y field component of the mode has a maximum near the center of the metal-dielectric interfaces, with a symmetric profile similar to that shown in Fig. 8. This suggests that the mode should be excitable using a simple end-fire technique similar to the one employed to excite surface plasmon-polariton modes;[19,6] this technique is based on maximizing the overlap between the incident field and that of the mode to be excited.

IV. MODE DISPERSION WITH FILM WIDTH

Since the modes supported by a metal film wave guide exhibit dispersion with film thickness, it is expected that they also exhibit dispersion with film width.

A. Modes supported by a metal film of width $w=0.5\,\mu$m

The study proceeds with the analysis of a metal film wave guide of width $w=0.5\,\mu$m. The material parameters and free-space wavelength that were used in the previous section were also used here. A film width of 0.5 μm was selected in order to determine the impact of a narrowing film on the modes supported and to demonstrate that the structure can still function as a wave guide though the free-space optical wavelength is greater than both the width and thickness of the film.

As in the previous section, the first eight modes supported by the structure (two for each symmetry listed in Table I) were sought, but in this case only six modes were found. The dispersion curves with thickness of the modes found are plotted in Fig. 10. The observations made in the previous section regarding the general behavior of the modes hold for other film widths, including this one.

The aa_b^2 and as_b^2 modes, which were the highest order modes found for a film of width $w=1$ μm, were not found in this case suggesting that the higher order modes ($m>0$) in general have a cutoff width. By comparing Fig. 10(a) with 2(a), it is apparent that decreasing the film width causes a decrease in the phase constant of the ss_b^1 and sa_b^1 modes, further supporting the existence of a cutoff width for these modes.

By comparing Figs. 10 and 2, it is noted that the modes which do exhibit cutoff thicknesses (the ss_b^m modes with $m>0$ and the as_b^m modes with $m \geqslant 0$), exhibit them at a larger thickness for a narrower film width. This makes it possible to design a wave guide supporting only one long-ranging mode (the ss_b^0 mode) by carefully selecting the film width and thickness.

B. Dispersion of the ss_b^0 mode with film width

The dispersion with thickness of the ss_b^0 mode is shown in Fig. 11 for numerous film widths in the range $0.25 \leqslant w \leqslant 1$ μm, illustrating the amount of dispersion in the mode properties that can be expected due to a varying film width. In all cases the ss_b^0 mode evolves with decreasing film thickness into the TEM wave supported by the background but this evolution occurs more rapidly for a narrower width. For a film of thickness $t=20$ nm, for example, from Fig. 11(a), the normalized phase constant of the mode supported by a film of width $w=1$ μm is about 2.05 while that of the mode supported by a film of width $w=0.25$ μm is already about 2.

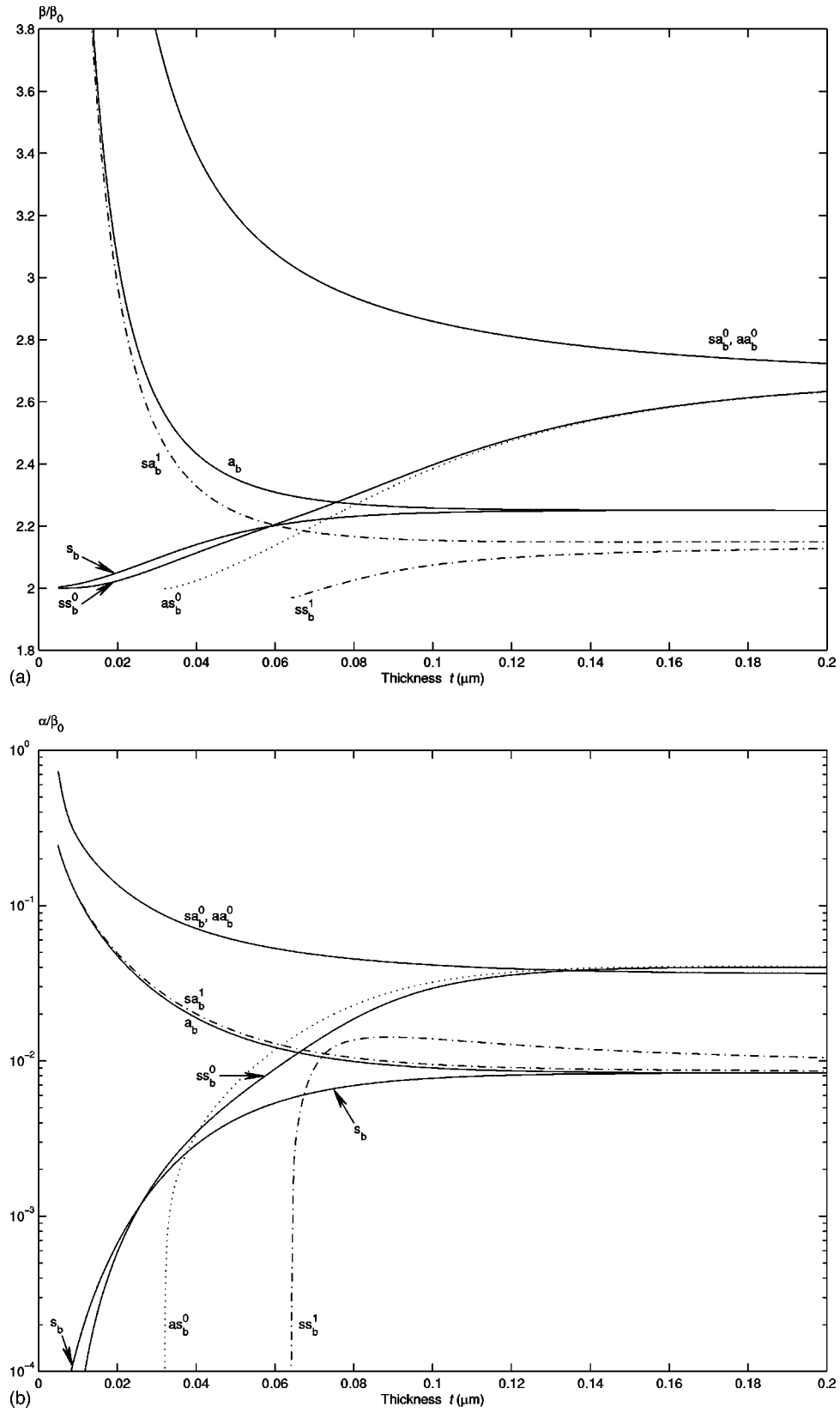

FIG. 10. Dispersion characteristics with thickness of the first six modes supported by a metal film wave guide of width $w=0.5\,\mu$m. The a_b and s_b modes supported for the case $w=\infty$ are shown for comparison. (a) Normalized phase constant. (b) Normalized attenuation constant.

This fact is also supported by the results plotted in Fig. 11(b) since the attenuation constant of the mode at a thickness of $t=20$ nm is closer to zero (the attenuation constant of the background) for narrow film widths compared to wider ones. Indeed, at a thickness of 10 nm, the attenuation of the mode for a width of $w=0.25\,\mu$m is more than an order of magni-

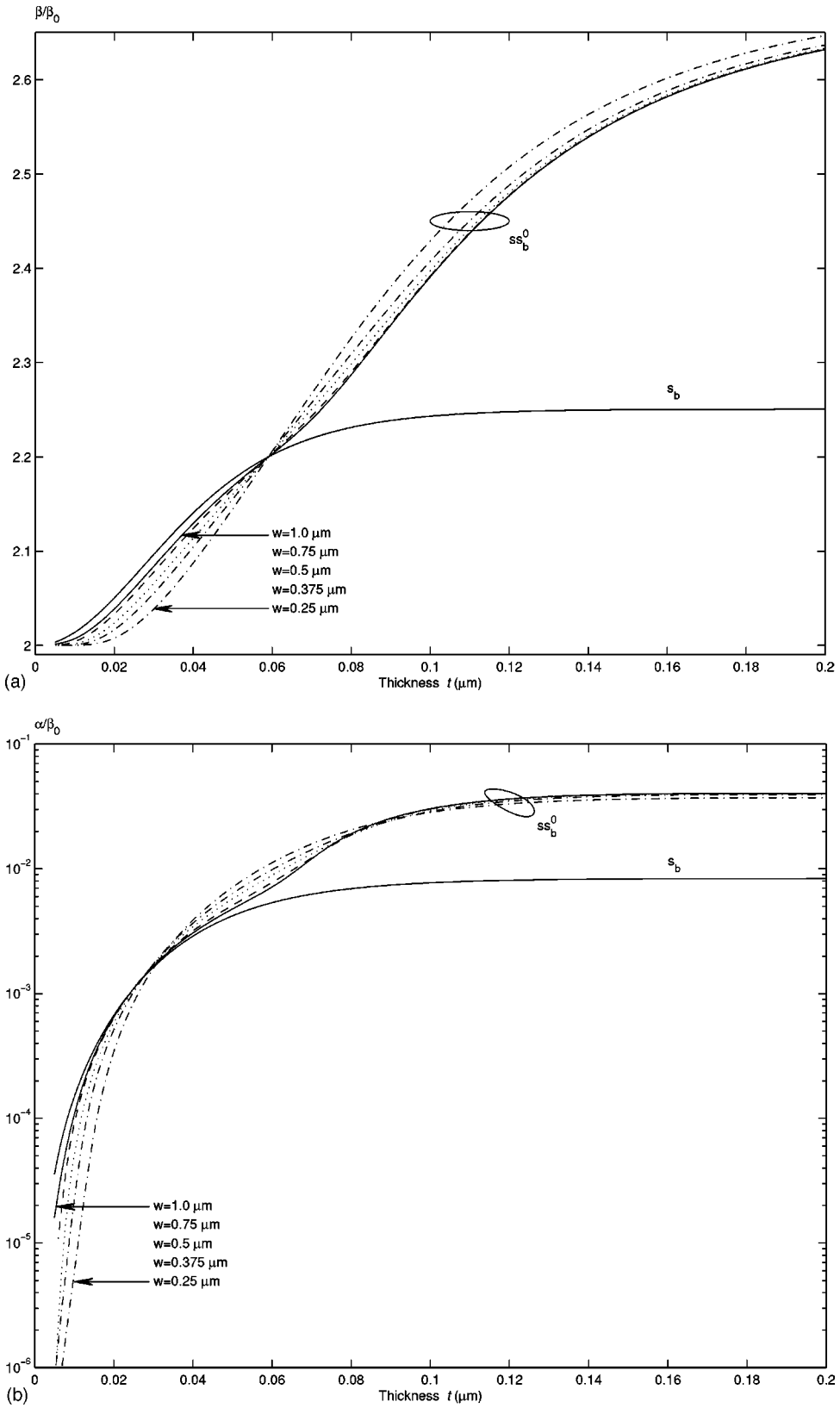

FIG. 11. Dispersion characteristics with thickness of the ss_b^0 mode supported by metal film wave guides of various widths. The s_b mode supported for the case $w=\infty$ is shown for comparison. (a) Normalized phase constant. (b) Normalized attenuation constant.

tude less than its attenuation at a width of $w=1\ \mu$m (and more than an order of magnitude less than that of the s_b mode supported by a metal film slab wave guide), indicating that this mode can be made even more long ranging by reducing both the film thickness and its width.

The dispersion of the mode with increasing film thickness also changes as a function of film width, as seen from Fig. 11(a). This is due to the fact that the amount of coupling between corners along the top and bottom edges increases as the film narrows, implying that the mode does not evolve

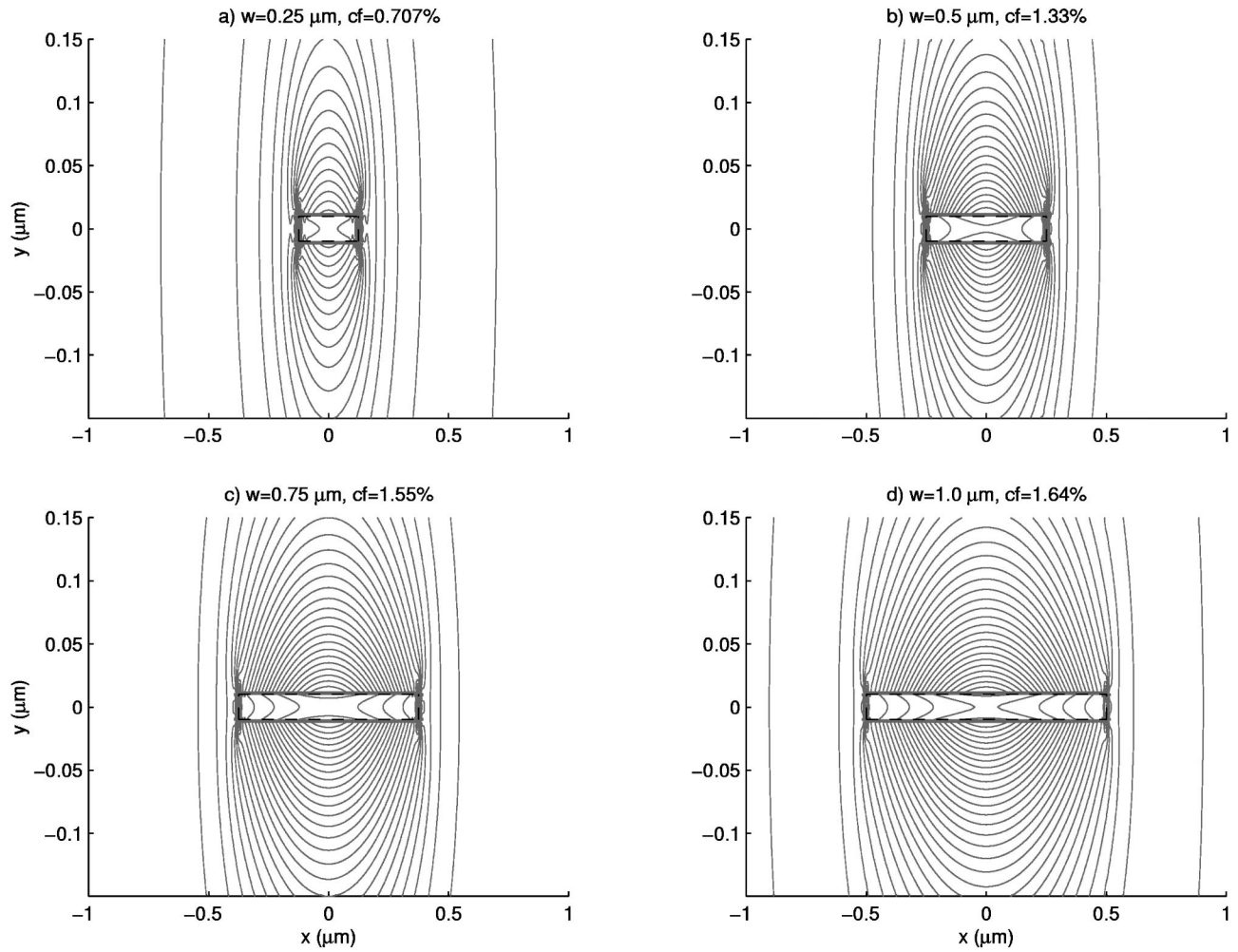

FIG. 12. Contour plot of $\mathrm{Re}\{S_z\}$ associated with the ss_b^0 mode for metal film wave guides of thickness $t=20\,\mathrm{nm}$ and various widths. The power confinement factor cf is also given in all cases, and is computed via Eq. (12) with the area of the wave guide core A_c taken as the area of the metal region. In all cases, the outline of the metal film is shown as the rectangular dashed contour.

with increasing thickness towards a plasmon-polariton mode supported by an isolated corner but rather towards a plasmon-polariton mode supported by the pair of corners coupled via these edges.

Figure 12 shows contour plots of $\mathrm{Re}\{S_z\}$ related to the ss_b^0 mode supported by films of thickness $t=20\,\mathrm{nm}$ and various widths. The power confinement factor is also given for all cases, with the area of the wave guide core A_c taken as the area of the metal region. This figure clearly illustrates how the fields become less confined to the lossy metal as its width decreases, explaining the reduction in attenuation shown in Fig. 11(b) at this thickness. In addition, the confinement factor ranges from 1.64 to 0.707 % for the widths considered, further corroborating this fact. The fields are also seen to spread out farther, not only along the horizontal dimension but along the vertical one as well, as the film narrows. This indicates that the mode supported by a narrow film is farther along in its evolution into the TEM mode supported by the background, compared to a wider film of the same thickness. It is also clear from this figure that the trade off between mode confinement and attenuation must be made by considering not only the film thickness but its width as well.

V. EFFECTS CAUSED BY VARYING THE BACKGROUND PERMITTIVITY

The changes in the propagation characteristics of the ss_b^0 mode due to variations in the background permittivity of the wave guide are investigated in this section. Only the ss_b^0 mode is considered since the main effects are in general applicable to all modes.

In order to isolate the effects caused by varying the background permittivity, the width of the metal film was fixed to $w=0.5\,\mu\mathrm{m}$ and its permittivity as well as the optical free-space wavelength of analysis were set to the values used in the previous sections. The relative permittivity of the background $\epsilon_{r,1}$ is taken as the variable parameter.

The dispersion with thickness of the ss_b^0 mode is shown in Fig. 13 for some background permittivities in the range $1 \leqslant \epsilon_{r,1} \leqslant 4$. Figure 14 compares contour plots of $\mathrm{Re}\{S_z\}$ related to this mode for a film of thickness $t=20\,\mathrm{nm}$ and for the same set of background permittivities used to generate the curves plotted in Fig. 13. From Fig. 14, it is observed that reducing the value of the background permittivity causes a reduction in field confinement to the metal. This reduction in field confinement within the lossy metal in turn causes a

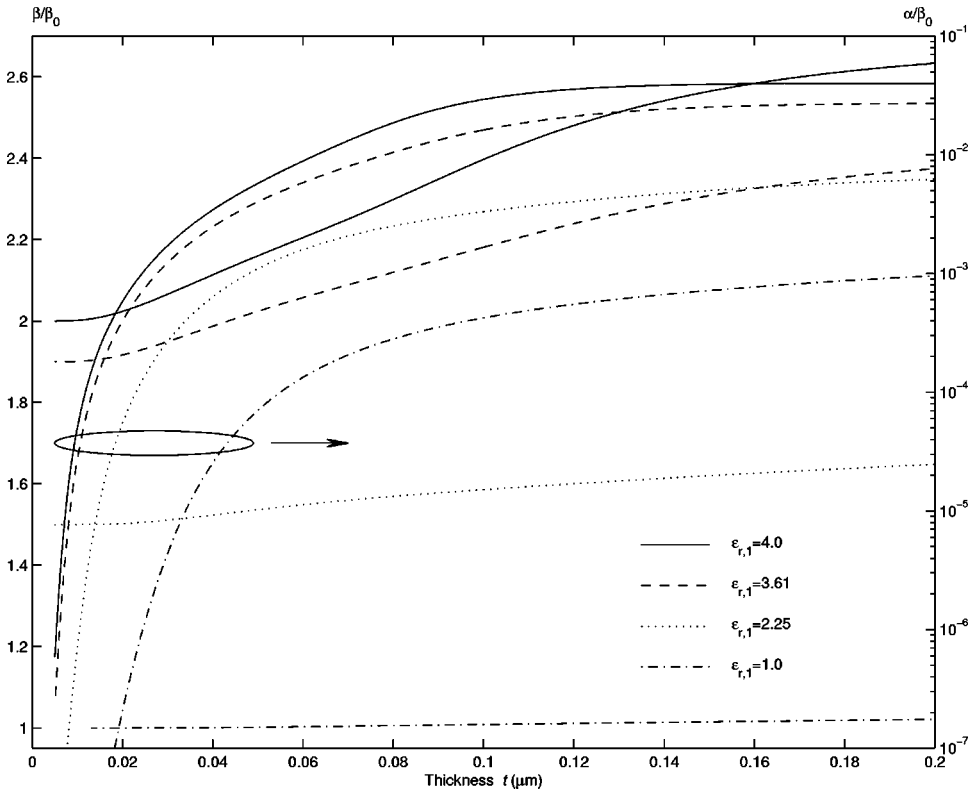

FIG. 13. Dispersion characteristics with thickness of the ss_b^0 mode supported by a metal film wave guide of width $w=0.5\,\mu$m for various background permittivities $\epsilon_{r,1}$. The normalized phase constant is plotted on the left axis and the normalized attenuation constant is plotted on the right one.

reduction in the attenuation of the mode that can be quite significant, Fig. 13 showing a reduction of almost four orders of magnitude at a film thickness of $t=20\,$nm, as the background relative permittivity ranges from $\epsilon_{r,1}=4$ to 1. It is also noted that the mode exhibits less dispersion with thickness as the background relative permittivity is reduced, since the normalized phase constant curves shown in Fig. 13 flatten out with a reduction in the value of this parameter.

From Fig. 14, it is seen that the mode power is confined to within approximately one free-space wavelength in all directions away from the film in all cases except (d), where fields are significant up to about two free-space wavelengths. In Fig. 14(c), the background permittivity is roughly that of glass and from Fig. 13 the corresponding normalized attenuation constant of the mode is about $\alpha/\beta_0=6.0\times10^{-5}$. The associated mode power attenuation in dB/mm, computed using the following formula:

$$\mathrm{Att}=\alpha\times\frac{20}{1000}\log_{10}(e) \tag{16}$$

is about 5 dB/mm. This value of attenuation is low enough and field confinement is high enough as shown in Fig. 14(c) to render this particular structure practical at this free-space wavelength for applications requiring short propagation lengths.

The changes in mode properties caused by varying the background permittivity as discussed above are consistent with the changes observed for the modes supported by a metal film slab wave guide and the observations are in general applicable to the other modes supported by a metal film of finite width. In the case of the higher order modes ($m>0$) and those exhibiting a cutoff thickness (the as_b^m modes for all m and the ss_b^m modes for $m>0$) additional changes in the mode properties occur. In particular, as the background permittivity is reduced, the cutoff width of the higher order modes increase as do all relevant cutoff thicknesses.

VI. FREQUENCY DEPENDENCE OF THE ss_b^0 MODE SOLUTIONS

In order to isolate the frequency dependence of the ss_b^0 mode solutions, the geometry of the metal film was held constant and the background relative permittivity was set to $\epsilon_{r,1}=4$. The relative permittivity of the metal film $\epsilon_{r,2}$ was assumed to vary with the frequency of excitation according to Eq. (1). In order to remain consistent with[6] the values $\omega_p=1.29\times10^{16}\,$rad/s and $1/\nu=\tau=1.25\times10^{-14}\,$s were adopted though the latter do not generate exactly $\epsilon_{r,2}=-19-j0.53$ at $\lambda_0=0.633\,\mu$m, which is the value used in the previous sections. This is due to the fact that values of ω_p and τ are often deduced by fitting Eq. (1) to measurements. The values used, however, are in good agreement with recent measurements made for silver[3] and are expected to generate frequency dependent results that are realistic and experimentally verifiable.

The dispersion characteristics of the ss_b^0 mode supported by films of width $w=0.5\,\mu$m and $w=1\,\mu$m, and thickness in the range $10\leqslant t\leqslant50\,$nm are shown in Fig. 15 for frequencies covering the free-space wavelength range $0.5\leqslant\lambda_0\leqslant2\,\mu$m. Curves for the s_b mode supported by metal film slab wave guides ($w=\infty$) of the same thicknesses are also shown for comparison.

The results given in Fig. 15(a) show in all cases that the normalized phase constant of the modes tend asymptotically towards that of the TEM wave supported by the background as the wavelength increases, and that the convergence to this value is steeper as the width of the film decreases (for a

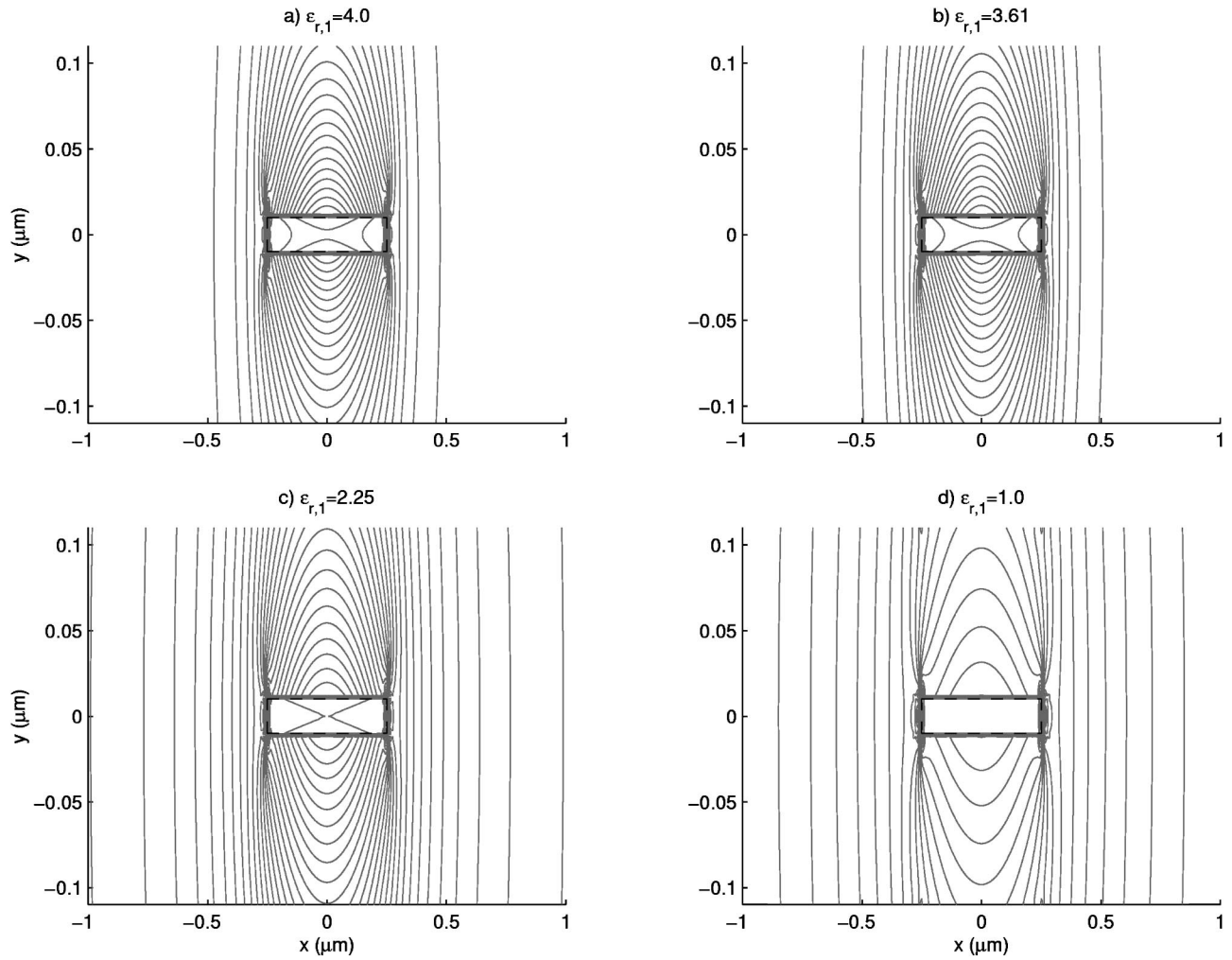

FIG. 14. Contour plot of $\mathrm{Re}\{S_z\}$ associated with the ss_b^0 mode for a metal film wave guide of width $w=0.5\,\mu$m and thickness $t=20$ nm for various background permittivities $\epsilon_{r,1}$. In all cases, the outline of the metal film is shown as the rectangular dashed contour.

given thickness). The curves remain essentially unchanged in character as the thickness changes but they shift upwards toward the top left of the graph with increasing thickness, as shown. Convergence to the asymptote value with increasing wavelength suggests that the ss_b^0 mode evolves into the TEM mode supported by the background. It is noteworthy that the ss_b^0 mode can exhibit very little dispersion over a wide bandwidth, depending on the thickness and width of the film, though flat dispersion is also associated with low field confinement to the metal film.

The results plotted in Fig. 15(b) show in all cases a decreasing attenuation with increasing wavelength and the curves show a sharper drop for a narrow film ($w=0.5\,\mu$m) compared to a wide one ($w=\infty$). The attenuation curves look essentially the same for all of the film thicknesses considered, though the range of attenuation values shifts downwards on the graph with decreasing film thickness.

Figure 16 gives contour plots of $\mathrm{Re}\{S_z\}$ related to the ss_b^0 mode for films of thickness $t=20$ nm and widths $w=0.5\,\mu$m and $w=1\,\mu$m, for three free-space wavelengths of operation: $\lambda_0=0.6$, 0.8, and 1.2 μm. Comparing the contours shown in Fig. 16, explains in part the frequency dependent behavior plotted in Fig. 15. Figure 16 shows that the mode power contours spread out farther from the film as the wavelength increases, which means that the mode confinement to the metal region decreases explaining in part the decrease in losses and the evolution of the mode towards the TEM mode of the background as shown in Fig. 15. This behavior is more pronounced for the waveguide of width $w=0.5\,\mu$m compared to the wider one of width $w=1.0\,\mu$m.

There are two mechanisms causing changes in the ss_b^0 mode as the frequency of operation varies. The first is the geometrical dispersion which changes the optical or apparent size of the film and the second is material dispersion which is modeled for the metal region using Eq. (1). If no material dispersion is present, then the geometrical dispersion renders the film optically smaller as the free-space wavelength is increased (an effect similar to reducing t and w) so in the case of the ss_b^0 mode, confinement to the film is reduced and the mode spreads out in all directions away from the latter. Now based on Eq. (1), it is clear that the magnitude of the real part of the film's permittivity $|\mathrm{Re}\{\epsilon_{r,2}\}|$ varies approximately in a $1/\omega^2$ or λ_0^2 fashion while the magnitude of its imaginary part $|\mathrm{Im}\{\epsilon_{r,2}\}|$ varies approximately in a $1/\omega^3$ or λ_0^3 fashion. However, an increase in $|\mathrm{Re}\{\epsilon_{r,2}\}|$ reduces the penetration depth of the mode fields into the metal region and combined with the geometrical dispersion causes a net

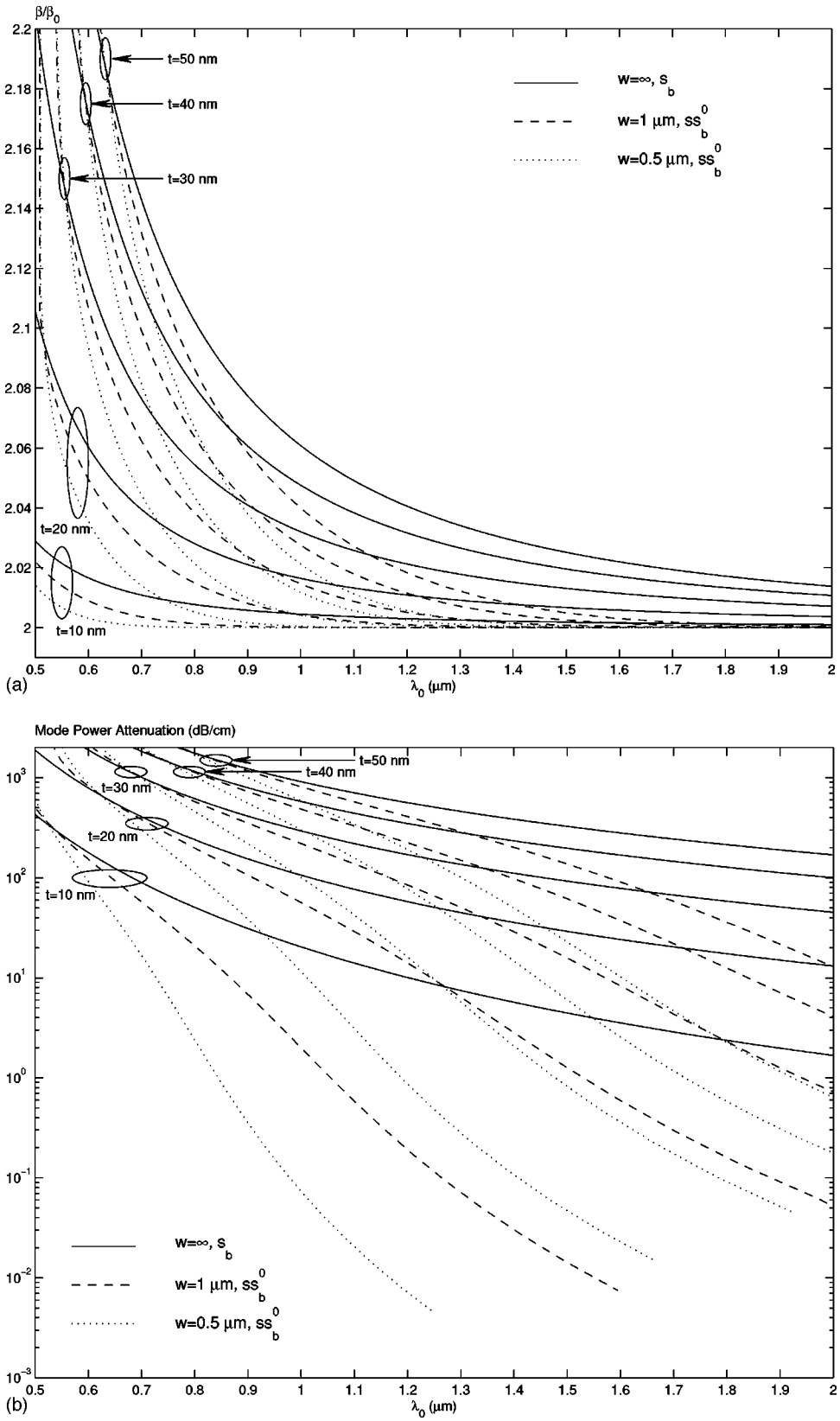

FIG. 15. Dispersion characteristics with frequency of the ss_b^0 mode supported by metal film wave guides of width $w=0.5\,\mu$m and $w=1\,\mu$m and various thicknesses t. The s_b mode supported for the case $w=\infty$ and the thicknesses considered is shown for comparison. (a) Normalized phase constant. (b) Mode power attenuation computed using Eq. (16) and scaled to dB/cm.

decrease in mode attenuation with increasing wavelength even though the losses in the film increase in a λ_0^3 fashion.

Figure 15(b) shows that mode power attenuation values in the range 0.1 to 10 dB/cm are possible near communications wavelengths ($\lambda_0 \sim 1.5\,\mu$m) using structures of reasonable dimensions: $w \sim 1.0\,\mu$m and $t \sim 15$ nm. Such values of attenu-

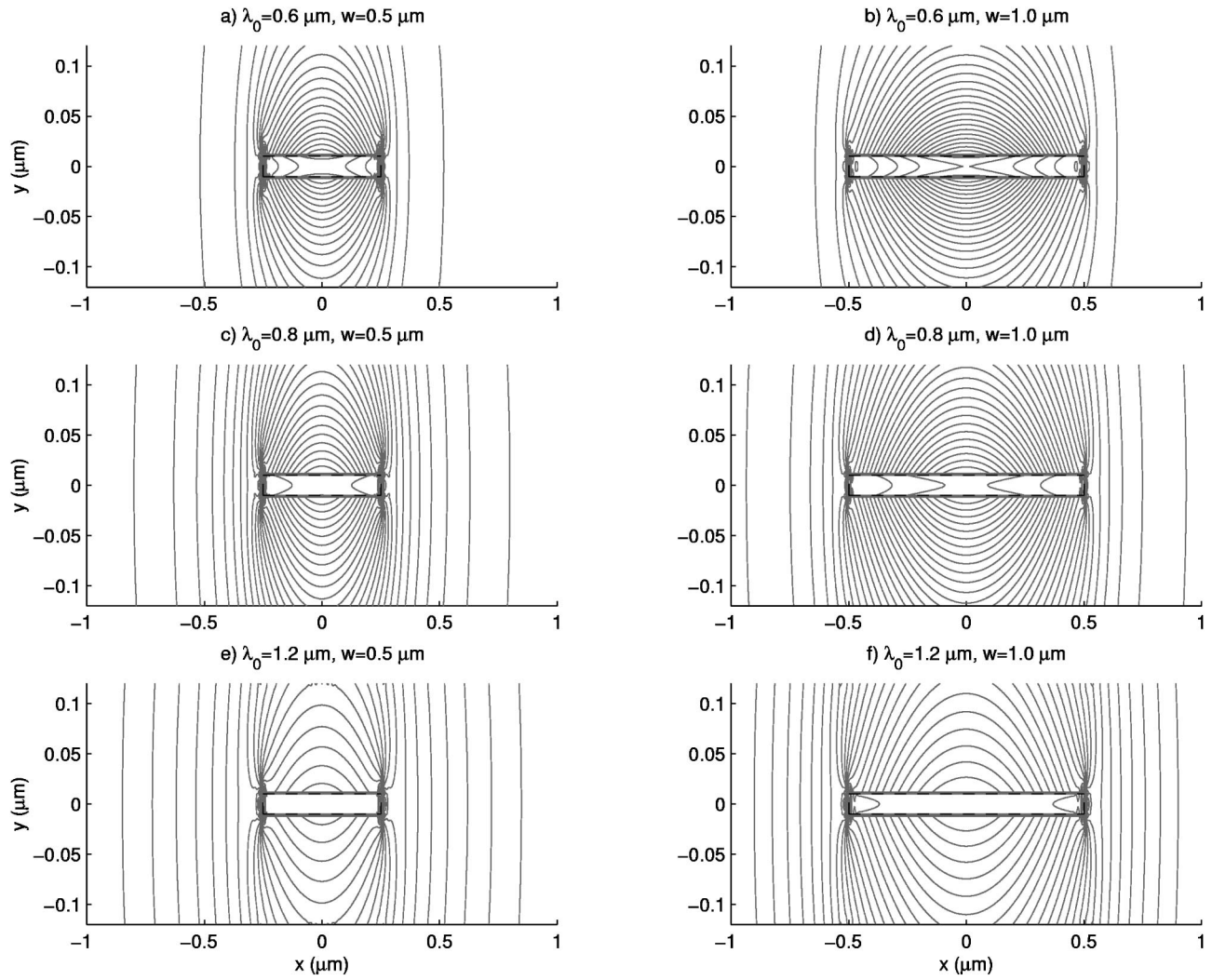

FIG. 16. Contour plot of $\mathrm{Re}\{S_z\}$ associated with the ss_b^0 mode for metal film wave guides of width $w=0.5\,\mu$m and $w=1\,\mu$m, and thickness $t=20$ nm at various free-space wavelengths of excitation λ_0. In all cases, the outline of the metal film is shown as the rectangular dashed contour.

ation are low enough to consider the ss_b^0 mode as being long ranging, suggesting that these wave guides are practical for applications requiring propagation over short distances. As shown in the previous section, even lower attenuation values are possible if the background permittivity is lowered. From parts (c) and (f) of Fig. 16 (case $\lambda_0=1.2\,\mu$m, which is near communications wavelengths), it is apparent that the mode power confinement is within one free-space wavelength of the film, which should be tight enough to keep the mode bound to the structure if a reasonable quality metal film of the right geometry can be constructed.

VII. CONCLUSION

The purely bound optical modes supported by a thin lossy metal film of finite width, embedded in an infinite homogeneous dielectric have been characterized and described. The modes supported by the structure are divided into four families depending on the symmetry of their mode fields and none of the modes are TM in nature (as they are in the metal film slab wave guide). In addition to the four fundamental modes that exist, numerous higher order modes are supported as well. A proposed mode nomenclature suitable for identifying them has been discussed. The dispersion of the modes with film thickness has been assessed and the behavior in general terms found to be consistent with that of the purely bound modes supported the metal film slab wave guide. In addition, it has been found that one of the fundamental modes and some higher order modes have cutoff thicknesses. Mode dispersion with film width has also been investigated and it has been determined that the higher order modes have a cutoff width, below which they are no longer propagated. The effect of varying the background permittivity on the modes has been investigated as well, and the general behavior found to be consistent with that of the modes supported by a metal film slab wave guide. In addition it was determined that the cutoff width of the higher order modes decreases with decreasing background permittivity and that all cutoff thicknesses are increased.

One of the fundamental modes supported by the structure, the ss_b^0 mode exhibits very interesting characteristics and is potentially quite useful. This mode evolves with decreasing film thickness towards the TEM wave supported by the background, (an evolution similar to that exhibited by the s_b

mode in metal film slab wave guides), its losses and phase constant tending asymptotically towards those of the TEM wave. In addition, it has been found that decreasing the film width can reduce the losses well below those of the s_b mode supported by the corresponding metal film slab wave guide. Reducing the background permittivity further reduces the losses. However, a reduction in losses is always accompanied by a reduction in field confinement to the wave guide core which means that both of these parameters must be traded off one against the other. Furthermore, carefully selecting the film's thickness and width can make the ss_b^0 mode the only long-ranging mode supported. It has also been demonstrated that mode power attenuation values in the range of 10 to 0.1 dB/cm are achievable at optical communications wavelengths with even lower values possible. Finally, the mode evolved into its most useful form, has a field distribution that renders it excitable using end-fire techniques.

The existence of the ss_b^0 mode as well as its interesting characteristics makes the finite-width metal film wave guide attractive for applications requiring short propagation distances. The wave guide offers 2D field confinement in the transverse plane rendering it useful as the basis of an integrated optics technology. Interconnects, power splitters, power couplers, and interferometers could be built using the guides. Finally the structures being quite simple should be inexpensive to fabricate.

*Fax: (613) 562-5175. Electronic address: berini@site.uottawa.ca

[1] *American Institute of Physics Handbook*, 3rd ed. (McGraw-Hill, New York, 1972).
[2] *Handbook of Optics* (McGraw-Hill, New York, 1978).
[3] D. J. Nash and J. R. Sambles, J. Mod. Opt. **43**, 81 (1996).
[4] A. D. Boardman, *Electromagnetic Surface Modes* (Wiley, New York, 1982).
[5] E. N. Economou, Phys. Rev. **182**, 539 (1969).
[6] J. J. Burke, G. I. Stegeman, and T. Tamir, Phys. Rev. B **33**, 5186 (1986).
[7] L. Wendler and R. Haupt, J. Appl. Phys. **59**, 3289 (1986).
[8] F. A. Burton and S. A. Cassidy, J. Lightwave Technol. **8**, 1843 (1990).
[9] B. Prade, J. Y. Vinet, and A. Mysyrowicz, Phys. Rev. B **44**, 13 556 (1991).
[10] P. Tournois and V. Laude, Opt. Commun. **137**, 41 (1997).
[11] W. Johnstone, G. Stewart, T. Hart, and B. Culshaw, J. Lightwave Technol. **8**, 538 (1990).
[12] M. Rajarajan, C. Themistos, B. M. A. Rahman, and K. T. V. Grattan, J. Lightwave Technol. **15**, 2264 (1997).
[13] P. Berini, Opt. Lett. **24**, 1011 (1999).
[14] R. Pregla and W. Pascher, in *Numerical Techniques for Microwave and Milimeter-Wave Passive Structures*, edited by T. Itoh (Wiley, New York, 1989).
[15] P. Berini and K. Wu, IEEE Trans. Microwave Theory Tech. **MTT-44**, 749 (1996).
[16] P. Berini, A. Stöhr, K. Wu, and D. Jager, J. Lightwave Technol. **14**, 2422 (1996).
[17] R. Culver, Brit. J. Appl. Phys. **3**, 376 (1952).
[18] R. C. Boonton, *Computational Methods for Electromagnetics and Microwaves* (Wiley, New York, 1992).
[19] G. I. Stegeman, R. F. Wallis, and A. A. Maradudin, Opt. Lett. **8**, 386 (1983).